Attosecond Electron Dynamics in Molecular Systems

Oliver G. Alexander

Blackett Laboratory Extreme Light Consortium, Physics Department, Imperial College London, SW7 2AZ, U.K.

Jon P. Marangos

Blackett Laboratory Extreme Light Consortium, Physics Department, Imperial College London, SW7 2AZ, U.K. (Corresponding Author)

Marco Ruberti

Blackett Laboratory Extreme Light Consortium, Physics Department, Imperial College London, SW7 2AZ, U.K.

Morgane Vacher

Nantes Université, CNRS, CEISAM, UMR 6230, F-44000 Nantes, France

---

Abstract

In this paper we review the topic of attosecond electron dynamics in molecular systems. We present a digest of recent research on this topic conducted by ourselves and other researchers with the intention of providing an accessible, but rigorous, account of the current state of this intriguing field of research. A short account of the background quantum theory is given before discussing recent theoretical advances on understanding correlation driven electron dynamics and electron nuclear coupling in molecules undergoing fast photoionisation. We then review experimental advances, using both high harmonic generation and XFEL based ultrafast x-ray pulses, and provide three recent case studies from our own work to illustrate this. The final sections look forward to the next steps in this field, we discuss the prospect for controlling attochemistry as well as extending attosecond measurement methods to electron dynamics in larger molecules and condensed phase systems.

Keywords: Ultrafast molecular science, attosecond, atto-chemistry, high harmonic generation, XFEL, charge migration, charge dynamics, X-ray absorption spectroscopy, electron-nuclear coupling, quantum control

Attosecond Electron Dynamics in Molecular Systems

Oliver G. Alexander

Blackett Laboratory Extreme Light Consortium, Physics Department, Imperial College London, SW7 2AZ, U.K.

Jon P. Marangos

Blackett Laboratory Extreme Light Consortium, Physics Department, Imperial College London, SW7 2AZ, U.K. (Corresponding Author)

Marco Ruberti

Blackett Laboratory Extreme Light Consortium, Physics Department, Imperial College London, SW7 2AZ, U.K.

Morgane Vacher

Nantes Université, CNRS, CEISAM, UMR 6230, F-44000 Nantes, France

---

Contents

1 Introduction **4**

2 Theory background **7**
- 2.1 Electronic structure and electronic dynamics 9
- 2.2 Coupled electron-nuclear dynamics 14

3 Theory of attosecond charge dynamics **17**
- 3.1 Electronic correlation and its manifestation 17
- 3.2 Electron-nuclear coupling 24
- 3.3 Coherence versus entanglement 27

4 Observations of attosecond molecular dynamics **33**
- 4.1 Pump-probe methodology for tracking electronic coherence . 33
- 4.2 High harmonic generation based attosecond measurements . . 34
- 4.3 Time-resolved x-ray spectroscopy and photoelectron spectroscopy 35

Preprint submitted to Advances in Atomic, Molecular and Optical PhysicsJanuary 25, 2023

4.4 Strong field pumps and probes 37
4.5 XFEL based few-femtosecond to attosecond domain measurements 38

5 Case studies **40**
5.1 Transient XAS in isopropanol 40
5.2 Electron-nuclear coupling in glycine 43
5.3 HHG spectroscopy in deutriated and protonated molecules . . 44

6 Quantum control and the concept of charge-directed reactivity **48**

7 Future directions of the field **53**
7.1 Emerging attosecond capabilities (XLEAP, angular streaking, nonlinear interactions) and techniques (liquid jets, transmitted spectrum) 53
7.2 Prospects for, and the importance of, studying attosecond dynamics in larger molecules, biomolecules, condensed phase systems 55
7.3 Prospects for, and the importance of, controlling chemistry. Can we control bimolecular reactions? 59

8 Conclusion **60**

1. Introduction

Ultrafast electronic dynamics driven by electromagnetic fields lie at the core of fundamental processes in nature, from vision through photosynthesis to radiation damage. They are also central to many technologies underpinning modern society, from photodetectors through photovoltaics to water-splitting. Despite their ubiquity much remains to be understood of the mechanisms that couple light to ultrafast electronic dynamics and the subsequent chemical and physical changes. Among the current unanswered question are: (i) How does pure electronic charge flow couple to nuclear structural dynamics? (ii) To what extent do quantum coherence of electronic and/or vibronic states play a role? and (iii) Is it possible to dynamically control the evolution of these quantum states to steer the outcome of the processes? In this article we discuss these questions, and some of the recent research that seeks the answers, by considering the case of molecules undergoing photoexcitation.

The timescales of electronic dynamics will typically be in the few- to sub-femtosecond range. This may not at first be obvious if, for instance, one considers an excited state lifetime in an isolated neutral atom. The fastest decay timescale is related to spontaneous emission arising from coupling to the vacuum field. This is relatively weak and takes place on typically nanosecond timescales. If, however, one considers the H atom in the Bohr model, one deduces a much faster semi-classical dynamics for the electron motion: the orbit time of an electron in the first Bohr orbit (the Bohr radius a_0) is set by the orbit circumference ($2\pi a_0 = 3.33 \times 10^{-10}$ m) and the velocity ($v = c/136$), which give an orbital period of only 1.5×10^{-16} s (i.e. 150 attoseconds).

Moving to a fully quantum description of a H atom let us consider a superposition of the n=1 and n=2 states (say the $1s$ and $2p$ states) with energies E_0 and $E_0 + \Delta E$. The wavefunction evolves with time, t, as:

$$|\psi(0,t)\rangle = \frac{1}{\sqrt{2}} e^{-iE_0 t/\hbar} \left(|1\mathrm{s}\rangle + e^{-i\Delta E t/\hbar} |2\mathrm{p}\rangle \right). \quad (1)$$

The expectation value of the radius,

$$\begin{aligned} \langle r \rangle &= \langle \psi(0,t)| \, r \, |\psi(0,t)\rangle \\ &= \frac{1}{2} \langle 1\mathrm{s}| \, r \, |1\mathrm{s}\rangle + \frac{1}{2} \langle 2\mathrm{p}| \, r \, |2\mathrm{p}\rangle + \cos\left(\frac{\Delta E}{\hbar} t - \phi \right) |\langle 1\mathrm{s}| \, r \, |2\mathrm{p}\rangle|, \quad (2) \end{aligned}$$

$\phi = \arg \langle 1\mathrm{s}| \, r \, |2\mathrm{p}\rangle$

where the first two terms vanish due to the symmetry of the wavefunction but the third term does not and oscillates with a periodicity set by $\hbar$ times the inverse of the energy separation of the states (approx. 10.2 eV = 1.63×10^{-18} J) i.e. a period of 64.4 attoseconds. The timescales of the variation of related "observables", such as charge density, that manifest oscillatory character due to the formation of superposition of electronic states will be similarly fast. For instance the period of oscillation of the charge density of a superposition of valence molecular states separated by 200 meV will oscillate with a period of 20 fs, whilst for an energetic separation of 2 eV this will be only 2 fs. The question we seek to address is: do electronic superpositions with these intrinsic attosecond/few-femtosecond timescales play a role in any chemically relevant phenomena?

As we will discuss, the nuclear part of the molecular wavefunction must also be considered to fully understand the dynamical response, as well as the coupling to chemical change associated with the rearrangements of the

atomic nuclei. This coupling profoundly affects the nature of the initial electronic superpositions. This is through both very rapid nuclear motion, e.g. the C-H bond vibrational period of around 30 fs, and through the nuclear geometry spread of the zero-point energy state that leads to a range of energy separations of the electronic superposition that causes a dephasing of the coherence. We will discuss this further in later sections, but the broad picture is that the coupling to the nuclear degrees of freedom can lead to vibronic excitation and to the dephasing/decoherence of the electronic system.

It is clear that with the current generation of few-femtosecond/attosecond light sources it is possible to prepare molecules in electronic state superpositions. The consequences of doing this will be discussed in this article. In particular, we argue that this gives an opportunity to explore new time-domain quantum coherence and to direct scenarios in chemistry that may even allow control over chemical reactions through dynamical manipulation of the coherence of the superposition. This is a timely and legitimate technical and scientific goal, although whether attosecond time domain chemistry becomes a new technological frontier is as yet unknown. Moreover, it addresses some of the fundamental issues of chemical physics as we must go beyond the Born-Oppenheimer approximation to understand how to treat both the electronic and nuclear parts of the dynamically evolving molecular quantum system.

Still more intriguing is the realisation that these scenarios may become relevant not just in our advanced laser technology. Indeed, the coupling of electronic charge flow to structural dynamics plays a key role in chemical reactivity and dynamical events in matter, for example, in all solar activated processes such as photosynthesis, photovoltaics, H generation from water splitting, vision etc. We thus ought to consider whether coherent electronic excitation can play a significant role in this wide array of natural and technological systems. Recent considerations of the coherent bandwidth of sunlight at the Earths surface suggest a coherent bandwidth equivalent to around 1 fs (or an energy bandwidth ≈ 2 eV) (Ricketti et al., 2022), raising the intriguing possibility that electronic superpositions may be formed by illumination of biomolecules by the Sun. Does this play any role in biochemical processes or even the evolution of life on Earth? Whilst we don't aspire to fully answer these questions we will attempt to illustrate the current knowledge around the subject of attosecond timescale electronic dynamics in molecules. In particular we will stress that, whilst an earlier claim of a role of long lived (> 100 fs) (Engel et al., 2007) electronic coherence in photomolecular process looks

unlikely (Scholes et al., 2017), current theoretical considerations, backed by recent experimental data, suggest that electronic coherence can survive for ≈ 10 fs in certain systems and may couple to longer lived vibronic coherence.

This article is arranged as follows:

First, in Section 2 we will introduce the theoretical framework for describing electron and nuclear dynamics and explain why the full computation of both electronic and nuclear states is in many cases beyond the limit of current computational tractability. We will also present the theoretical methods that aim to take into account electron correlation and non-adiabatic coupling.

In Section 3 we will discuss some of the key predictions from the available theory: how electronic coherence can manifest in various types of charge migration, how the electron-nuclear coupling affects electron dynamics, and the fundamental question of how in a multi-part quantum system quantum coherence competes with quantum entanglement.

Next, in Section 4, we turn to the diverse different experimental methodologies: pump-probe scheme, high harmonic generation spectroscopy, time-resolved x-ray and photoelectron spectroscopy, strong-field schemes and XFEL based measurements.

Section 5 follows with the evidence so far obtained, illustrating two recent experiments on charge migration in x-ray ionized isopropanol and glycine, and an earlier example of ultrafast coupled electron-nuclear dynamics following strong field ionization of methane.

In Section 6, we then address the prospects for control of molecular processes through manipulating the electronic coherence.

In Section 7 we will examine the emerging experimental possibilities, the application to measurements in large molecules and condensed phase systems and the approaches to controlling bimolecular reactions.

We do not attempt a comprehensive review of all the available literature, but do try to provide the reader with our own perspective on this developing topic. This will be illustrated by our own and other relevant recent works. We hope that this article will prove of utility to researchers in the field and to others wishing to find out more about and enter the area.

2. Theory background

The advancement of attosecond technology requires theoretical and computational tools capable to simulate and predict correlated many-body dynamics in atoms and molecules on time-scales which range from hundreds of

attoseconds up to tens of femtoseconds. The theoretical framework for the description of the quantum dynamics on these ultrafast time-scales is based on the time-dependent Schrödinger equation (Schrödinger, 1926):

$$i\hbar\frac{\partial}{\partial t}\Phi(\mathbf{x},\mathbf{R},t) = \hat{H}(\mathbf{r},\mathbf{R})\Phi(\mathbf{x},\mathbf{R},t) \tag{3}$$

which models the time evolution, as driven by the Hamiltonian operator $\hat{H}(\mathbf{r},\mathbf{R})$, of a quantum system comprising M atomic nuclei and N electrons, with a total wavefunction expressed by

$$\Phi(\mathbf{x},\mathbf{R},t) = \Phi(\mathbf{x}_1,\mathbf{x}_2,...,\mathbf{x}_N,\mathbf{R}_1,\mathbf{R}_2,...,\mathbf{R}_M,t), \tag{4}$$

where $\mathbf{x} = (\mathbf{r}, \mathbf{s})$ and $\mathbf{R}$ denote the position and spin of the electrons and the nuclear coordinates, respectively.

The non-relativistic Hamiltonian of a general, interacting many-body system comprising electrons and nuclei can be written as

$$\begin{aligned}\hat{H}(\mathbf{r},\mathbf{R}) = &-\sum_{I=1}^{M}\frac{1}{2m_I}\nabla_I^2 - \sum_{i=1}^{N}\frac{1}{2}\nabla_i^2 - \sum_{i=1}^{N}\sum_{I=1}^{M}\frac{Z_I}{|\mathbf{r}_i-\mathbf{R}_I|} + \\ &+\sum_{i=1}^{N}\sum_{j>i}^{N}\frac{1}{|\mathbf{r}_i-\mathbf{r}_j|} + \sum_{I=1}^{M}\sum_{J>I}^{M}\frac{Z_I Z_J}{|\mathbf{R}_I-\mathbf{R}_J|}\end{aligned} \tag{5}$$

where Z_I and m_I are the electric charge and mass, respectively, of the I-th nucleus, $|\mathbf{r}_i - \mathbf{r}_j|$ and $|\mathbf{R}_I - \mathbf{R}_J|$ are the inter-electron and inter-nuclear distances, respectively. The first and second terms on the right hand side of Eq. (5) represent the kinetic energy operators of the nuclei and of the electrons, respectively, from now on denoted as $\hat{T}_n(\mathbf{R})$ and $\hat{T}_e(\mathbf{r})$. The third term describes the Coulomb attraction between the nuclei and electrons, while the last two terms represent the repulsive Coulomb interaction between the electrons and between the nuclei, respectively. For these last two terms the sum over the second electron or nucleus is restricted so as to avoid double counting.

Non-relativistic quantum mechanics is mostly adopted in the field to describe the attosecond dynamics of many-electron systems. It is worth noting that the validity of the non-relativistic approximation requires one to work with light (low-Z) atoms, and compounds thereof (a category of which includes most organic molecules), as well as photoelectrons with kinetic energy up to the few-keV limit.

2.1. Electronic structure and electronic dynamics

At this stage, it is possible to just consider the solutions at a fixed set of nuclear coordinates ($\mathbf{R}$) and adopt the so-called *frozen-nuclei approximation*. The latter relies on the assumption that, due to their much larger mass, nuclear motion takes place on a longer timescale than the motion of the lighter electrons. When this is the case, it is possible to consider the electrons as interacting with a force field generated by a static alignment of the nuclei and safely neglect the nuclear kinetic energy term in the Hamiltonian of Eq. (5). It is worth noting that also the term describing the repulsion between the nuclei can be discarded in the frozen-nuclei approximation, as its only contribution is to add a constant negative contribution to the eigenenergies, with no effect on the corresponding eigenstates. The so-called *electronic* or *frozen-nuclei* Hamiltonian can then we written as

$$\hat{H}_e(\mathbf{r};\mathbf{R}) = -\sum_{i=1}^{N}\frac{1}{2}\nabla_i^2 - \sum_{i=1}^{N}\sum_{I=1}^{M}\frac{Z_I}{|\mathbf{r}_i-\mathbf{R}_I|} + \sum_{i=1}^{N}\sum_{j>i}^{N}\frac{1}{|\mathbf{r}_i-\mathbf{r}_j|}\,. \tag{6}$$

The solution of the electronic time-independent Schrödinger equation,

$$\hat{H}_e(\mathbf{r};\mathbf{R})\Psi_i(\mathbf{r};\mathbf{R}) = E_i(\mathbf{R})\Psi_i(\mathbf{r};\mathbf{R}) \tag{7}$$

for any given nuclear geometry $\mathbf{R}$, defines $\{\Psi_i(\mathbf{r};\mathbf{R})\}$ the electronic eigenstates, also called the *adiabatic electronic states*, and $\{E_i(\mathbf{R})\}$ the electronic eigenvalues. These quantities depend on the nuclear positions $\mathbf{R}$ in a parametric way. In particular, the parametric dependence of the electronic energy on the position of the nuclei gives rise to the concept of the so-called *adiabatic potential energy surfaces*. Each adiabatic electronic state has its own corresponding potential energy surface (PES), a function that depends on the $3M-6$ nuclear degrees of freedom.

In order to find the energy eigenstates corresponding to the electronic Hamiltonian of Eq. 6, it is necessary to engineer suitable approximations that simplify the mathematical problem to be solved, but at the same time give qualitatively as well as quantitatively accurate results. In the following we will briefly outline the theoretical framework of quantum chemical, wavefunction based methods. The target quantity of this class of methods is the $3N$-dimensional many-body wavefunction of the system, where N is the total number of electrons.

The simplest form of such a N-electron wavefunction consists of the antisymmetrized product of N different single-electron orbitals, the so-called

Slater determinant:

$$\Psi\left(\mathbf{x}_1, \mathbf{x}_2, ..., \mathbf{x}_N; t\right) = \frac{1}{\sqrt{N!}} \begin{vmatrix} \psi_1\left(\mathbf{x}_1\right) & \psi_2\left(\mathbf{x}_1\right) & ... & \psi_N\left(\mathbf{x}_1\right) \\ \psi_1\left(\mathbf{x}_2\right) & \psi_2\left(\mathbf{x}_2\right) & ... & \psi_N\left(\mathbf{x}_2\right) \\ .... & ... & ... & ... \\ \psi_1\left(\mathbf{x}_N\right) & \psi_2\left(\mathbf{x}_N\right) & ... & \psi_N\left(\mathbf{x}_N\right) \end{vmatrix} \tag{8}$$

where the columns and rows of the matrix are labelled by the orbitals and the electron number, respectively. The Slater determinant is a linear combination of simple products, i.e. $\psi_1\left(\mathbf{x}_1\right)\psi_2\left(\mathbf{x}_2\right)\ldots\psi_N\left(\mathbf{x}_N\right)$, which is anti-symmetric with respect to the exchange of any two electrons and thus satisfies the Pauli exclusion principle:

$$\Psi\left(\mathbf{x}_2, \mathbf{x}_1, ..., \mathbf{x}_N; t\right) = -\Psi\left(\mathbf{x}_1, \mathbf{x}_2, ..., \mathbf{x}_N; t\right) . \tag{9}$$

Solutions in the form of single Slater-determinants are formally correct for one-body Hamiltonians, i.e. scenarios in which the electrons would behave as independent particles. The electronic Hamiltonian in Eq. 6 can be split into a one-body term

$$\hat{H}^1(\mathbf{r}; \mathbf{R}) = -\sum_{i=1}^{N}\left[\frac{1}{2}\nabla_i^2 + \sum_{I=1}^{M}\frac{Z_I}{|\mathbf{r}_i - \mathbf{R}_I|}\right] . \tag{10}$$

that is summed over all the electrons in the system, and a two-body interaction term

$$\hat{H}^2(\mathbf{r}; \mathbf{R}) = +\sum_{i=1}^{N}\sum_{j>i}^{N}\frac{1}{|\mathbf{r}_i - \mathbf{r}_j|} . \tag{11}$$

The simplest approximation consists of completely neglecting the term in Eq. 11, and working with the one-body potential given by Eq. 10. This approximation is, however, too crude. A better approximation, designed for calculating the electronic ground state, consists of finding the best one-body Hamiltonian which minimises the energy of the single Slater-determinant solution (Szabo and Ostlund, 1996) and takes into account the presence of the two-body term of Eq. 11. This is the so-called Hartree-Fock (HF) Hamiltonian:

$$\hat{f}\left(\mathbf{r}\right) = -\sum_{i=1}^{N}\left[\frac{1}{2}\nabla_i^2 + \sum_{I=1}^{M}\frac{Z_I}{|\mathbf{r}_i - \mathbf{R}_I|}\right] + \hat{J}_N\left(\mathbf{r}\right) + \hat{K}_N\left(\mathbf{r}\right) , \tag{12}$$

$$\hat{f}\left(\mathbf{r}\right)\psi_j\left(\mathbf{x}\right) = \epsilon_j\,\psi_j\left(\mathbf{x}\right) .$$

Within the HF theory, the N electrons can be effectively considered as independent particles that move in the HF mean-field potential, the latter also approximating their mutual repulsion. The second term $\hat{J}_N(\mathbf{r})$ in the HF potential is the direct Coulomb term, a local term that describes repulsion from the negative charge density generated by the other $N-1$ electrons:

$$\hat{J}_N(\mathbf{r})\,\psi_i(\mathbf{x}) = + \sum_{j=1}^{N} \int \frac{\psi_j^*(\tilde{\mathbf{x}})\,\psi_j(\tilde{\mathbf{x}})}{|\tilde{\mathbf{r}}-\mathbf{r}|} d^4\tilde{\mathbf{x}}\ \psi_i(\mathbf{x})\ . \tag{13}$$

The third term $\hat{K}_N(\mathbf{r})$ is the non-local exchange term, which originates from the anti-symmetric nature of the Slater determinant solution:

$$\hat{K}_N(\mathbf{r})\,\psi_i(\mathbf{x}) = - \sum_{j=1}^{N} \int \frac{\psi_j^*(\tilde{\mathbf{x}})\,\psi_i(\tilde{\mathbf{x}})}{|\tilde{\mathbf{r}}-\mathbf{r}|} d^4\tilde{\mathbf{x}}\ \psi_j(\mathbf{x})\ . \tag{14}$$

This last term has the effect of depleting the charge density in the immediate vicinity of the electron. Note that the term $j = i$ is included in both summations of Eqs. 13,14, as they cancel each other out.

Since the Fock operator of Eq. 12 has a functional dependence on the solution itself, Eq. 12 is solved by an iterative process and the resulting field is usually called self consistent field (SCF). Among the set of converged orbitals, the lowest energy ones are filled with electrons to form the Hartree-Fock ground state for the system, denoted as Ψ_0^{HF}. These orbitals are usually called occupied orbitals, while HF molecular orbitals (MOs) that are unoccupied in the HF ground state are called virtual orbitals.

Once the HF ground state of the neutral system has been determined, all the possible Slater determinants of the neutral system can be classified into the excitation classes:

$$\left[|\Psi^N\rangle\right] = \left[|1h1p\rangle = \hat{a}_p^\dagger \hat{a}_h |\Psi_0^{HF}\rangle;\ |2h2p\rangle = \hat{a}_{p_1}^\dagger \hat{a}_{p_2}^\dagger \hat{a}_{h_1} \hat{a}_{h_2} |\Psi_0^{HF}\rangle;\ ...;\ |NhNp\rangle\right] . \tag{15}$$

In Eq. 15, the annihilation $\hat{a}_h$ and creation $\hat{a}_p^\dagger$ operators create a hole and a particle, respectively, in the HF electronic ground state. The class of determinants that are equivalent to the ground state apart from one electron that is placed in a virtual orbital are called one-hole-one-particle (1h1p) excited determinants.

Analogously, for the cationic system, all the possible Slater determinants can be classified using the HF molecular orbital of the neutral system by

using the following classes:

$$\left[|\Psi^{N-1}\rangle\right] = \left[|1h\rangle = \hat{a}_h|\Psi_0^{HF}\rangle;\ |2h1p\rangle = \hat{a}_{p_1}^{\dagger}\hat{a}_{h_1}\hat{a}_{h_2}|\Psi_0^{HF}\rangle;\ ...;\ |Nh(N\text{-}1)p\rangle\right]. \tag{16}$$

In order to go beyond the HF approximation, we can rewrite the many-electron Hamiltonian of Eq. 6 as the sum of the one-body HF component of Eq. 12 and a new two-body component that describes the residual mutual interaction between electrons that is not taken into account within the mean-field description.

$$\hat{H}_e(\mathbf{r};\mathbf{R}) = \hat{f}(\mathbf{r}) + \left[\sum_{i=1}^{N}\sum_{j>i}^{N}\frac{1}{|\mathbf{r}_i - \mathbf{r}_j|} - \hat{J}_N(\mathbf{r}) - \hat{K}_N(\mathbf{r})\right]. \tag{17}$$

The effects of this residual inter-particle interaction are usually referred to as *electron correlation*. Highly accurate many-electron wavefunctions and transition matrix elements are routinely obtained by the post-Hartree-Fock (post-HF) methods of *ab initio* quantum chemistry (Szabo and Ostlund, 1996). These methods describe electron correlation by addressing the effects of the second term in square brackets in Eq. 17 and are based on the use of finite sets of square-integrable, typically Gaussian type orbitals (GTO), single-electron basis functions.

One possibility is to diagonalize the total Hamiltonian of Eq. 17 on a truncated Hilbert space consisting of all the possible Slater determinants up to some maximum excitation class (see Eqs. 15,16). This type of approach is called configuration interaction (CI). The first term $\hat{f}(\mathbf{r})$ is diagonal in the basis of Eqs. (15,16), as the Slater determinants of the various excitation classes are constructed with HF molecular orbitals. Truncating the size of the excitation classes for the neutral molecule to 1h1p or to 2h2p configurations yields what is referred to as configuration interaction singles (CIS) and doubles (CISD), respectively. As an illustrative example, the block structure of the CISD Hamiltonian matrix for a neutral molecule reads as

$$\mathbf{H}^{CISD} = \begin{pmatrix} E_{HF} & 0 & H_{0,2h2p} \\ 0 & H^{CIS}_{1h1p,1h1p} & H_{1h1p,2h2p} \\ H_{2h2p,0} & H_{2h2p,1h1p} & H_{2h2p,2h2p} \end{pmatrix}, \tag{18}$$

where the first diagonal block refers to the HF ground state. The main drawback to these methods is size inconsistency: within any truncated CI calculation, the total energy of two sufficiently separated, non-interacting

systems is not exactly equivalent to the sum of their respective energies, separately calculated at the same level of approximation.

A more advanced, from-first-principles technique to describe correlated many-electron systems, is the algebraic diagrammatic construction (ADC) methodology (Schirmer, 2018). ADC has been vastly successful as an *ab initio* quantum chemical method for calculating the energies and properties of ionized and excited electronic states in polyatomic molecules (Kissin et al., 2021). Similarly to CI, a general ADC scheme involves an expansion in excitation classes, but unlike the CI expansion, an nth order scheme in the ADC(n) hierarchy of approximation uses a perturbation-theoretically corrected (rather than Hartree-Fock) reference state

$$|\Psi_0^{ADC(n)}\rangle = |\Psi_0^{HF}\rangle + |\Psi_0^{MP(1)}\rangle + |\Psi_0^{MP(2)}\rangle + ... + |\Psi_0^{MP(n)}\rangle\,. \tag{19}$$

In the expansion of Eq. 19, which is referred to as Moller-Plesset perturbation expansion (Szabo and Ostlund, 1996), the perturbation term is considered to be the residual interaction of Eq. 17. This approach yields a more compact, size-consistent representation of the many-electron wavefunctions (Schirmer, 2018). As an illustrative example, the block structure of the ADC(2) Hamiltonian matrix for a neutral N-electron system reads as

$$\mathbf{H}^{ADC(2)} = \begin{pmatrix} E_{MP(2)} & 0 & 0 \\ 0 & \tilde{H}^{(2)}_{1h1p,1h1p} & H^{(1)}_{1h1p,2h2p} \\ 0 & H^{(1)}_{2h2p,1h1p} & H^{(0)}_{2h2p,2h2p} \end{pmatrix}, \tag{20}$$

where the numbers in parenthesis denote the maximum order of perturbation theory in the expansion of the matrix elements corresponding to each block. The off-diagonal 1h1p-2h2p blocks are calculated at first order and thus coincide with the ones of the CISD theory (Eq. 18).

Finally, we would like to mention another class of methods that combine the SCF procedure with CI, i.e. where both the coefficients of the molecular orbitals on the single-electron basis set functions, and the ones of the total many-electron wavefunction on the configuration state functions, are determined within the same variational calculation. This class of methods is referred to as Multiconfiguration SCF (MC-SCF). A particular version of such methods is the so-called Complete Active Space SCF (CAS-SCF), where a full CI is restricted to a subset (n) of the total number of electrons in the system, as well as to a subset (m) of the total MOs, referred to as active space (Szabo and Ostlund, 1996).

2.2. Coupled electron-nuclear dynamics

In the general case, one can express the total molecular wavefunction in the complete basis of electronic eigenstates:

$$\Phi(\mathbf{r},\mathbf{R},t) = \sum_{i}^{\infty} \chi_i(\mathbf{R},t)\Psi_i(\mathbf{r};\mathbf{R}) \tag{21}$$

The ansatz (21) is called the Born-Huang expansion and is exact in the limit of complete basis. The expansion coefficients $\{\chi_i(\mathbf{R},t)\}$ depend on time and can be interpreted as time-dependent nuclear wavepackets on electronic states $\{\Psi_i(\mathbf{r};\mathbf{R})\}$.

When inserting (21) into (3), multiplying on the left by $\Psi_j^*(\mathbf{r};\mathbf{R})$ and integrating over $\mathbf{r}$, one obtains the equation of motion for the time-dependent nuclear wavepackets:

$$i\hbar\frac{\partial}{\partial t}\chi_j(\mathbf{R},t) = [\hat{T}_n(\mathbf{R}) + E_j(\mathbf{R})]\chi_j(\mathbf{R},t) + \sum_{i}^{\infty} \hat{\Lambda}_{ji}\chi_i(\mathbf{R},t) \tag{22}$$

The first term on the right hand side of (22) corresponds to the nuclear quantum dynamics on a given single electronic state $\Psi_j(\mathbf{r};\mathbf{R})$ while the second term is responsible for the coupling between the nuclear wavepacket $\chi_j(\mathbf{R},t)$ on state $\Psi_j(\mathbf{r};\mathbf{R})$ and the nuclear wavepackets $\chi_i(\mathbf{R},t)$ on the other electronic states. The non-adiabatic coupling operator is the sum of the kinetic coupling (scalar quantity) and derivative coupling (vectorial quantity):

$$\hat{\Lambda}_{ji} = \sum_A \frac{-\hbar^2}{2m_A}[\langle\Psi_j|\nabla_A^2\Psi_i\rangle + 2\langle\Psi_j|\nabla_A\Psi_i\rangle\nabla_A] \tag{23}$$

with m_A the mass of nucleus A. The Born-Oppenheimer approximation consists of neglecting all $\hat{\Lambda}_{ji}$ based on the fact that nuclei are heavy particles (Born et al., 1955): $m_A \gg 1$. It allows one to simulate nuclear dynamics on a single adiabatic potential energy surface:

$$i\hbar\frac{\partial}{\partial t}\chi_j(\mathbf{R},t) = [\hat{T}_n(\mathbf{R}) + E_j(\mathbf{R})]\chi_j(\mathbf{R},t) \tag{24}$$

To understand when the Born-Oppenheimer approximation breaks down, one needs to look at the numerator of equation (23):

$$\hat{\Lambda}_{ji} \propto \langle\Psi_j|\nabla_A\Psi_i\rangle = \frac{\langle\Psi_j|\nabla_A\hat{H}_e|\Psi_i\rangle}{E_i - E_j} \tag{25}$$

The non-adiabatic couplings become large when two electronic eigenstates come close in energy. Geometries where different PES become degenerate are known as conical intersections. They play an important role in non-radiative de-excitation transitions from excited electronic states to the ground electronic state of molecules. As an example of such dynamics, one can cite the case of the DNA molecule which remains stable after UV irradiation because of the presence of a conical intersection that induces a non-radiative transition back to the molecule's electronic ground state (Kang et al., 2002).

Equation (22) cannot be solved exactly. Instead, one uses the *group* Born-Oppenheimer approximation considering the non-adiabatic couplings within a group of electronic states and neglecting the coupling with electronic states outside this group.

In practice, one needs a way to express the nuclear wavefunctions $\{\chi_i(\mathbf{R})\}$. Standard grid-based quantum mechanical simulations are expensive computationally because of their exponential scaling with the system size. They are thus often limited to few nuclear coordinates. Using the MCTDH method (Worth et al., 2008), one can afford more nuclear coordinates. This method involves the development of a model Hamiltonian, typically based on harmonic potentials, and a reduced number of nuclear coordinates. A separate bottleneck is the computation and fitting of the potential energy surfaces prior to any dynamics calculation.

"On-the-fly" dynamics methods have been developed to address these issues (Vacher et al., 2016b). They are direct dynamics methods since the potential energy surfaces are calculated as needed along trajectories avoiding the pre-requirement of globally fitted surfaces, and sampling only the relevant regions of the potential energy surfaces. These nuclear trajectories are used to describe the nuclear wavepacket motion, i.e. the nuclear wavepacket is expanded in the basis of nuclear trajectories via expansion coefficients. The several on-the-fly methods able to describe non-adiabatic dynamics treat the electrons quantum mechanically. The major feature that differentiates them is the treatment of the nuclear motion through the basis trajectories. Do the basis trajectories obey quantum or classical mechanics? Are the basis trajectories coupled or independent? Does each basis trajectory evolve on a single potential energy surface (at a time) or does it follow the gradient of a superposition of electronic states and therefore evolve on an effective potential energy surface? This last point raises an important distinction. In the former case, a different set of basis trajectories is used for each electronic state. In technical terms, a *multi-set* formalism is used. In the latter case,

one set of basis trajectories is used to treat the dynamics in all electronic states: a *single-set* formalism is used. Using attosecond technology, one can populate several electronic states simultaneously and coherently. For this reason, the single-set class of methods seems more natural since each nuclear trajectory "feels" all populated electronic states.

The simplest single-set dynamics method is the Ehrenfest method (Ehrenfest, 1927; Vacher et al., 2014b). In the latter, a time-dependent electronic wavefunction is defined and expanded in the basis of electronic eigenstates: $\Psi(\mathbf{r},t;\mathbf{R}) = \sum_i c_i(t)\Psi_i(\mathbf{r};\mathbf{R})$. Electron dynamics are described quantum mechanically by solving the time-dependent electronic Schrödinger equation:

$$i\hbar\frac{\partial c_j(t)}{\partial t} = c_j(t)E_j(\mathbf{R}) - i\hbar\sum_{i,A} c_i(t)\langle\Psi_j|\nabla_A\Psi_i\rangle\cdot\frac{d\mathbf{R}_A}{dt} \tag{26}$$

The nuclear wavepacket is described using an ensemble of independent classical trajectories. Each follows the gradient of a superposition of electronic states, i.e. evolves on an effective potential energy surface:

$$\frac{d\mathbf{P}_A}{dt} = -\nabla_A\langle\Psi(\mathbf{r},t;\mathbf{R})|\hat{H}_e(\mathbf{r};\mathbf{R})|\Psi(\mathbf{r},t;\mathbf{R})\rangle \tag{27}$$

with $\mathbf{P}_A$ the classical momentum of nuclei A. One deficiency of the Ehrenfest method (i.e. of independent classical mean-field trajectories) is that the nuclear motion is bound to be the same for all electronic states. This could lead to non-physical asymptotic behaviours. The Ehrenfest method is thus expected to be valid at short times before the nuclear wavepackets belonging to different electronic states move too far apart from each other. By treating the nuclear motion classically, the spatial delocalisation of the nuclear wavepacket is in principle lost. To recover this, one uses the ensemble of trajectories with initial sampled classical nuclear positions $\mathbf{R}$ and momenta $\mathbf{P}$ to mimic the nuclear wavepacket distribution. Wigner sampling, for instance, can reproduce the distribution of the quantum vibrational ground state (in the harmonic approximation) of the ground state species before photo-excitation/ionisation (Wigner, 1932).

The direct dynamics variational multi-configuration Gaussian (DD-vMCG) method is an on-the-fly single-set dynamics method which treats quantum mechanically both electron and nuclear dynamics (Richings et al., 2015; Vacher et al., 2016b). It describes the nuclear wavepacket using a basis set of time-dependent Gaussian basis functions (GBF) $\{g_i(\mathbf{R},t)\}$. The total

molecular wavefunction reads:

$$\Phi(\mathbf{r},\mathbf{R},t) = \sum_{i\epsilon g}\sum_{G} a_G^i g_G(\mathbf{R},t)\Psi_i(\mathbf{r};\mathbf{R}) \tag{28}$$

The GBF evolve quantum mechanically and are variationally coupled, meaning that the time evolution of not only the GBF expansion coefficients is determined by the time-dependent Schrödinger equation,

$$i\hbar\frac{d\mathbf{a}^j}{dt} = \mathbf{S}^{-1}\cdot[\ (\mathbf{H}^{jj} - i\hbar\mathbf{T})\cdot\mathbf{a}^j + \sum_i \mathbf{H}^{ji}\cdot\mathbf{a}^i] \tag{29}$$

but also of their parameters $\{\lambda_{G,A}\}$, eg. mean position and momentum (collected in the vector Λ):

$$i\hbar\frac{d\Lambda}{dt} = \mathbf{C}^{-1}\mathbf{Y} \tag{30}$$

$$C_{GA,HB} = \sum_i \rho_{GH}^{ii}(S_{GH}^{AB} - [\mathbf{S}^{A0}\cdot\mathbf{S}^{-1}\cdot\mathbf{S}^{0B}]_{GH}) \tag{31}$$

$$Y_{GA} = \sum_{i,j}\sum_{H} \rho_{GH}^{ij}(H_{GH}^{ij,A0} - [\mathbf{S}^{A0}\cdot\mathbf{S}^{-1}\cdot\mathbf{H}^{ij}]_{GH}) \tag{32}$$

with $\hat{H}^{ji} = \langle\Psi_j|\hat{H}|\Psi_i\rangle$, $H_{GH}^{ji} = \langle g_G|\hat{H}^{ji}|g_H\rangle$ and $H_{GH}^{ij,A0} = \langle\frac{\partial g_G}{d\lambda_{G,A}}|\hat{H}^{ij}|g_H\rangle$ the Hamiltonian matrix elements, $S_{GH} = \langle g_G|g_H\rangle$, $S_{GH}^{A0} = \langle\frac{\partial g_G}{d\lambda_{G,A}}|g_H\rangle$ and $S_{GH}^{AB} = \langle\frac{\partial g_G}{d\lambda_{G,A}}|\frac{\partial g_H}{d\lambda_{H,B}}\rangle$ the overlap matrix elements, $T_{GH} = \langle g_G|\frac{dg_H}{dt}\rangle$ the time-derivative matrix elements and $\rho_{GH}^{ij} = a_G^{i*}a_H^j$ the density matrix elements.

It is noted that the non-adiabatic coupling (derivative coupling) presents a singularity at the point of degeneracy between electronic adiabatic states (Equation 25). This may cause problems in numerical simulations. Such problem can be avoided by working in a different basis of electronic states where the electronic Hamiltonian is not necessarily diagonal but where the nonadiabatic coupling is zero. Such a basis is called a *diabatic* basis (Delos and Thorson, 1979).

3. Theory of attosecond charge dynamics

3.1. Electronic correlation and its manifestation

As discussed in the previous section, in molecular systems each electron moves in the combined potential created by the ionic core and all other

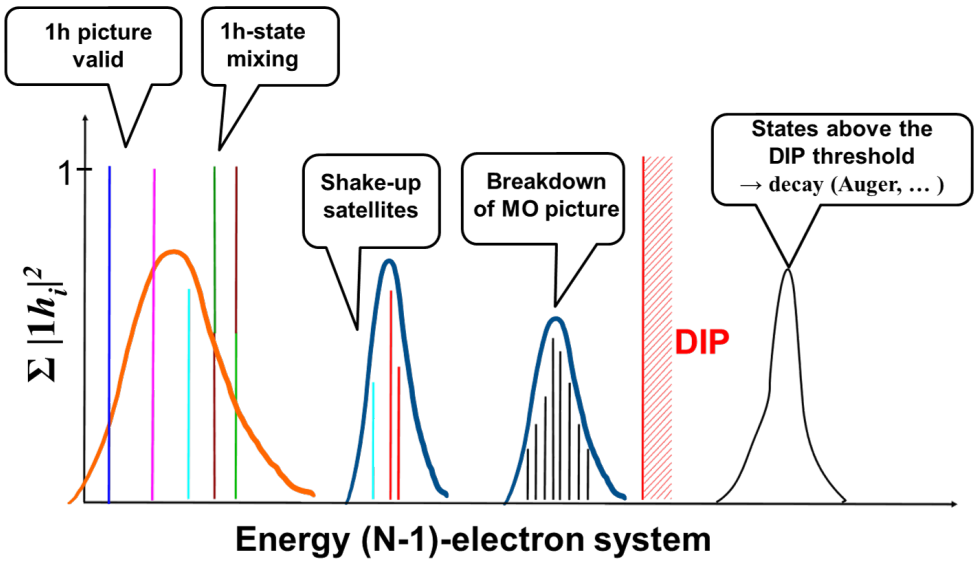

Figure 1: Typical electronic energy spectrum of a polyatomic molecular cation. In this schematic representation, each vertical line corresponds to an energy eigenstate of the cationic system; the height of each line corresponds to the so-called spectral intensity of the state, i.e. the sum of its squared coefficients on all the possible $1h_i$ configurations, $|1h_i|^2$. Contributions from different 1h configurations are shown with different colours. Typical bandwidth of ultrashort laser pulses capable of, by photoionizing the corresponding neutral molecule, coherently excite ionic states in the outer-valence (orange curve) and inner-valence (blue curves) energy region are also shown. Reproduced from Ref. (Ruberti et al., 2022) with permission from the Royal Society of Chemistry.

electrons. The electrons interact with each other while they move on the attosecond timescale. Electron correlation is thus a key component to understand both the structure and the ultrafast dynamics in a molecule, as they emerge under the influence of interatomic interactions between the electrons.

A typical electronic energy spectrum of a molecular cation in the fixed-nuclei approximation, extending beyond the double ionization potential (DIP) threshold, is shown in Figure 1. Each vertical line in the spectrum corresponds to an eigenstate of the electronic Hamiltonian (see subsection 2.1) of the cation and is located at the corresponding ionization energy ($E_n^{N-1} - E_0^N$). The height of each line corresponding to any given eigenstate, the so-called spectral intensity, reflects the contribution of the one-hole (1h) configurations to the ionic states and is given by the sum of their squared coefficients on all the possible $1h_i$ configurations, $\sum_i |C_{1h_i}^n|^2$. In the absence of electron

correlation one obtains a series of lines with a maximum height of 1, each corresponding to one of the HF molecular orbitals occupied in the HF electronic ground state of the molecule. This situation is the one that is usually referred to as Koopman's law, and is strictly valid only in the cases where electron correlation is negligible. This is often accurate in the outer-valence energy region, i.e. close to the first ionization potential (IP) of the system. As the energy of the ionic states increases, i.e. as electrons lying in deeper shells molecular orbitals start to be excited, electron correlation becomes more important. As a result, we start to observe all sorts of deviations from the Koopman's law: these can either be in the form of (1h)-mixing, where eigenstate are linear combinations of different 1h states, or lead to the formation of shake-up satellites and ultimately, in the inner-valence energy region to the complete breakdown of the molecular orbital (MO) picture (Figure 1).

In terms of electronic configurations, description of electron correlation in the modelling of the molecular cation requires one to include all the ionic two-hole - one-particle (2h-1p) configurations. This is done, for example, within the advanced descriptions given by the second (ADC(2)x) and third (ADC(3)) order methods of the ADC hierarchy (Schirmer, 2018). Electron correlation manifests itself in individual many-electron states of a molecular cation as a reduction of the spectral intensity line height (with the "missing" part reflecting the contribution of 2h1p configurations) and, related with the latter, as the appearance of additional (satellite) lines in the spectrum. A 2h1p configuration indeed describes the removal of an electron from a particular molecular orbital accompanied by the excitation of another electron to an initially unoccupied orbital.

Here it is important to remark that the role of 2h1p configurations is not only to take into account electron correlation, i.e. shake-up states, but also to model the electronic relaxation. The latter happens due to the change, with respect to the neutral molecule, in the mean-field potential that each electron experiences upon creation of a hole in a deeply-bound orbital.

The emergence of large-bandwidth, photoionizing laser sources (more details on this in Section 4) based on the high-order harmonic generation (HHG) (Johnson et al., 2018) and x-ray free electron laser (FEL) technologies (Duris et al., 2020), which have been actively developed over the recent two decades, has been instrumental in allowing one to produce, in principle arbitrary, coherent linear superpositions of such states in molecules using light-matter interaction. This has been a crucial step forward which dramatically increased the realm of physical scenarios accessible with respect to experiments based

on traditional narrow-bandwidth synchrotron radiation, which are mainly limited to addressing the properties of individual, incoherently populated eigenstates of the ionized system.

The new-generation attosecond light pulses can coherently excite and probe a system of interest over a broad range of photon energies and allow one to explore new, spectacular physical effects which result from the non-stationary quantum superpositions of ionized molecular states, such as molecular *hole migration* (Breidbach and Cederbaum, 2003).

The hole migration effect can be more easily understood starting with the following concept: if photoionization of a molecule in the inner-valence energy region consisted of a complete removal of an electron from the corresponding inner-shell molecular orbital, i.e. $|\Psi_i^{N-1}\rangle = \hat{a}_i |\Psi_0^N\rangle$ (the so-called sudden ionization limit), then a non-stationary, coherent linear superposition of electronic energy eigenstates of the cation would actually be populated as a result of electron correlation, i.e. the energy eigenstates with a non-zero amplitude on the 1h configuration corresponding to the created hole $|\Psi_i^{N-1}\rangle = \sum_{J=1}^{n} |C_{1h_i}^J|^2 |\Psi_{E_J}^{N-1}\rangle$. In the aforementioned sudden ionization picture, a high frequency pulse impulsively "destroys" an electron by removing it from one of the occupied MOs in the inner-valence energy region. This is an approximation for the state of the parent ion produced by photoionization, and its validity strictly requires the photon energy to be much higher than the ionization thresholds of the system. This idea was further explored by Cederbaum and co-workers in the early 2000's, and it was predicted that the ultrafast electron dynamics accompanying the coherent superposition of such molecular ionic eigenstates can, in large-enough polyatomic molecules, feature a back-and-forth migration of the positive charge across the molecular-ion backbone, on a sub- to few-femtosecond (fs) timescale. On longer timescales, this purely electronic coherent dynamics is potentially subject to decoherence (Despré et al., 2015; Vacher et al., 2017) due to coupling to the slower nuclear motion degree of freedom, which acts as a bath and could eventually lead to the final localization of the positive charge (see subsection 3.2).

"*Hole migration*" is a pure manifestation of electron correlation and assumes a coherent superposition of all the states resulting from the removal of an electron from a specific occupied orbital of the molecular ground state. However, in principle, other time-dependent coherent superpositions can be created by photoionizing a molecule. In the XUV and soft X-ray regimes several deeply-bound electronic states, i.e. higher excited states of the parent

ion, can be accessed by absorption of a single or a few photons. Within single-photon absorption, coherence between different single holes in the outer-valence part of the spectrum, where the energy separation between the different ionic states can be of the order of a few eV, typically requires ultra-short, attosecond laser pulses with a time duration of the order of hundreds of attoseconds. In the inner-valence energy region, longer pulses in the few-femtoseconds range can already be capable of exciting coherently either a single hole and its shake-up satellite states, or a series of correlated states in a breakdown of the MO picture scenario (see Figure 1). This is because of the higher density of states in the inner-valence energy region.

The state of the parent ion is described by the so-called reduced ionic density matrix (R-IDM). This is obtained by tracing the photoelectron subsystem out from the total electronic density matrix of the system

$$\hat{\rho}^{R-IDM}(t) = Tr^{e^-}\left(\hat{\rho}(t)\right), \tag{33}$$

where the partial trace has been performed on the degrees of freedom representing the photoelectron. In fact, for a photoionized system, at least at times t when the photoelectron is sufficiently far away from the parent ion, one of the electronic degrees of freedom (the one that will be identified as pertaining to the photoelectron) is associated to single-electron states that are physically distinguishable (e.g. for energy/momentum and spatial separation) from the ones occupied by the remaining (N-1) electrons.

Even when the complete, N-electron system is described by a pure state, i.e. $\hat{\rho}(t) = |\Psi^N(t)\rangle\langle\Psi^N(t)|$, the partial trace operation yields in general a mixed quantum state for the resulting parent ion sub-system. Representing the operator of Eq. (33) in the basis of eigenstates of the cationic Hamiltonian $|E_m^{N-1}\rangle$ we obtain:

$$\hat{\rho}^{R-IDM}(t) = \sum_{m,n} \rho_{m,n}^{R-IDM}(R,t)\, |E_m^{N-1}\rangle\langle E_n^{N-1}|. \tag{34}$$

The time-dependent populations P_m of each ionic eigenstate $|E_m^{N-1}\rangle$ is given by the corresponding diagonal matrix element, $P_m(t) = \rho_{m,m}^{R-IDM}(t)$, while the time-dependent degrees of coherence $G_{m,n}$ and relative phases $\phi_{m,n}$ between any pair of such states are given by

$$G_{m,n}(t) = \frac{|\rho_{m,n}^{R-IDM}(t)|}{\sqrt{P_m(t) \times P_n(t)}} \tag{35}$$

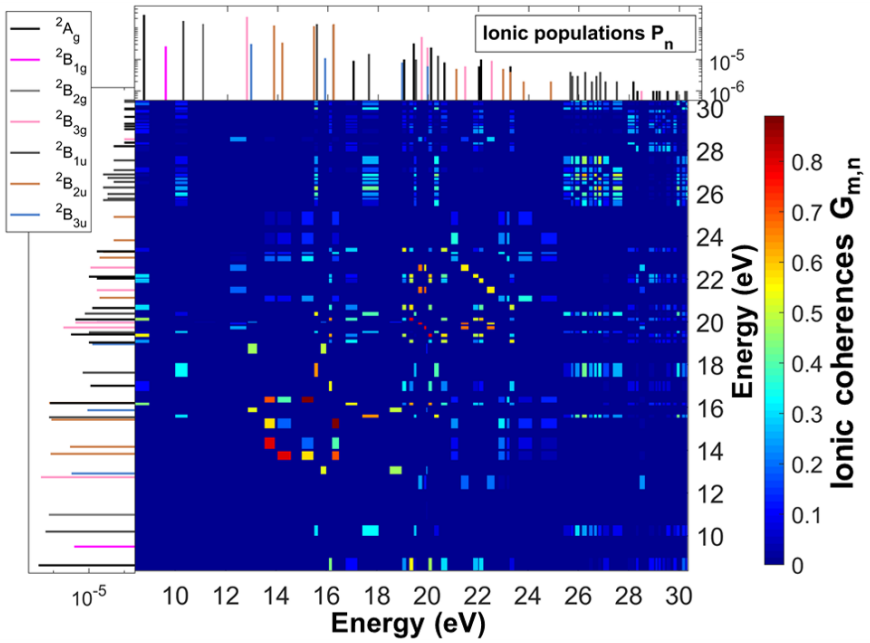

Figure 2: Quantum electronic coherence $G_{m,n}$ between the many-electron states populated by attosecond XUV photoionization of the pyrazine $C_4H_4N_2$ molecule. The ionic states were calculated using the RCS-ADC(2)x method and a cc-pVDZ basis set. The photoionization dynamics of pyrazine, interacting with a 25 eV attosecond XUV pulse linearly polarized along the N-N axis on the molecular plane and with a 7.5 eV FWHM spectral bandwidth, was simulated using the time-dependent (TD) version of the B-spline RCS-ADC(2)x method. The populations upon photoionization of the various ionic states are also shown in the vertical and horizontal side panels; different stick colours correspond to ionic states of different molecular point group symmetry, 2Ag (black), 2B1g (magenta), 2B2g (grey), 2B3g (pink), 2B1u (dark grey), 2B2u (brown), 2B3u (blue). Adapted from Ref. (Ruberti, 2021) with permission from the Royal Society of Chemistry.

and

$$\phi_{m,n}(t) = arg\left(\rho_{m,n}^{R-IDM}(t)\right), \tag{36}$$

respectively. Knowledge of the R-IDM (or equivalently the set of quantities in Eqs (35, 36)) constructed on the full electronic spectrum of the ionic subsystem, including bound excitations and highly-excited Auger-active states decaying on the fs timescale, allows one to reconstruct the ultrafast coherent electron dynamics that can be triggered by the photoionization process in the parent molecular ion.

In spite of the perturbative nature of the photoionization process at these shorter wavelengths (at least for laser intensity of the order of 10^{15} W/cm^2 or less), calculation of the quantum electronic coherences in the ionic sub-system requires an accurate treatment of electron correlation effects, which dominate in the inner-valence energy region of the ionic spectrum. Moreover, things are made complicated also by the high density of states in the region close to the DIP threshold and by the fact that each of these states of the parent ion has to be coupled to a continuum of states for the photoelectron sub-system. All these aspects make the accurate prediction of the reduced ionic density matrix upon attosecond XUV ionization of a polyatomic molecule very challenging.

These challenges have been in most part overcome by the recent development of sophisticated *ab initio* methods for ultrafast many-electron dynamics in polyatomic molecules (for a compact review see Ref. (Armstrong et al., 2021)), such as the time-dependent (TD) B-spline rescrited correlation space (RCS)-ADC (Ruberti, 2019a), which extends the *ab initio* ADC approach, originally developed to describe bound state dynamics, to the realm of ultrafast ionization dynamics. To accurately describe photoelectron continuum states, for which the traditional GTOs functions are badly suited (Ruberti et al., 2013, 2014b), the TD B-spline ADC technique (Ruberti et al., 2014a; Averbukh and Ruberti, 2018) relies on the use of B-splines - piecewise polynomial functions that accurately describe the strong oscillatory behaviour of continuum electronic wavefunctions far from the molecular region. This technique allows one to accurately describe both atomic and molecular bound-continuum dynamics in a series of diverse scenarios (Simpson et al., 2016; Ruberti et al., 2018a,b; You et al., 2019), combining the accurate description of electron correlation of quantum chemistry with the full account of the continuum dynamics of the photo-electron.

Moreover, the B-spline RCS-ADC method is based on the following ansatz for the many-electron wavefunction, expressed as a sum of bound/localized and ionization-channel components,

$$|\Psi^N_{RCS-ADC}(t)\rangle = |\Psi^N_0\rangle + \sum_I \sum_{h,p \in RCS} C_{Ih-Ip}(t)\, |\Psi^{N(ADC)}_{Ih-Ip}\rangle + \\ + \sum_{\gamma \in IS} \sum_m C_{\gamma,m}(t)\, \hat{a}^\dagger_\gamma\, |\Psi^{N-1(ADC)}_m\rangle \tag{37}$$

where the total single-electron orbital space (indexed by h, p, γ) has been separated into correlation ($h, p \in$ RCS) and ionization ($\gamma \in$ IS) spaces. In

Eq. 37, the index I and the index m represent different bound excitations classes and different ADC ionic eigenstates, respectively, while the $\hat{a}_\gamma^\dagger$ is a creation operator for the photoelectron represented in the IS orbital space. B-spline RCS-ADC naturally bridges the gap between multi-configurational *ab initio* techniques and closed-coupling schemes based on a limited number of essential, physically relevant ionic states, combining the key advantages of both, and allowing one to model, at a higher level of accuracy, the ionization of much larger polyatomic systems than previously possible. This type of computational capability allows one to accurately predict the mixed state of the ionized system prepared by attosecond ionization of a molecular system (Ruberti, 2019b, 2021). Complete theoretical characterization of the atto-ionized many-electron state and photo-induced attosecond charge dynamics is achieved by calculating the R-IDM for the bipartite ion-photoelectron system, with inclusion of the correlated shake-up states. As an illustrative example, in Figure 2 we show the degrees of quantum electronic coherence $G_{m,n}$, as calculated using the TD B-spline RCS-ADC method, between the electronic states of the pyrazine cation populated by attosecond XUV photoionization of the pyrazine neutral molecule (Ruberti, 2021).

3.2. Electron-nuclear coupling

As explained in the above sections, hole migration is a purely electronic phenomenon, i.e. it occurs even if the nuclei are fixed in space. Because of this and because of the expected difference in the timescale of electronic and nuclear motions, the effect of the nuclei on electron dynamics was overlooked in the first age of attochemistry (Nisoli et al., 2017). In practice, electron dynamics was typically simulated at a single and fixed nuclear geometry (Cederbaum and Zobeley, 1999; Remacle and Levine, 2007). Some of the purposes of our work have been to investigate the validity of the *fixed-nuclei* and *single-geometry* approximations used in most early theoretical studies.

To understand the extent to which neglecting nuclear motion is a reasonable approximation, we have simulated pure electron dynamics (with fixed nuclei) and electron dynamics with coupled nuclear motion using the Ehrenfest method, for a number of different molecular systems (Mendive-Tapia et al., 2013; Vacher et al., 2014b,a, 2015b; Jenkins et al., 2016a,b). Comparing the two types of simulations, the differences can be attributed to nuclear motion. We illustrate this here with the example of modified bismethyleneadamantanes (BMA) (Vacher et al., 2016a). The modified species contain

altered numbers of carbon atoms in the rings. We use a pair of integers, each indicating the number of carbon atoms in two of the four rings. Using this convention, the original BMA molecule corresponds to BMA[6,6]. We consider here the following modified molecules: BMA[5,5] (Figure 3a), BMA[6,5] and BMA[6,7]. Vertical valence ionization of the π system in these molecules takes place at geometries near the conical intersections between ground and first excited states of their cations. For the electronic structure, the complete active space self-consistent field (CASSCF) method with the 4 π orbitals in the active space and a 6-31G* basis set is used. We have calculated the (partitioned) electronic spin density - which locates the unpaired electron - as a tool to follow the electron dynamics.

The evolution of the partitioned spin densities with fixed nuclei and nuclei moving are shown with solid and dashed lines in Figures 3b-d, respectively. The electronic structure is not altered significantly by the modification to the adamantane cage: the nature of the initial localization and dynamics of the spin density of the electronic wavepacket is very similar for all three molecules, i.e. back and forth oscillations between the two methylene groups (Figure 3a). However, the electron dynamics is faster in BMA[5,5] cation (period of $\approx$ 5 fs with fixed nuclei, Figure 3b) than in BMA[6,5] cation ($\approx$ 15 fs, Figure 3c) and BMA[6,7] cation ($\approx$ 37 fs, Figure 3d). This is because the energy gap between the populated electronic states is larger in the former. Comparing the electron dynamics results obtained with fixed nuclei and nuclei moving, we see that the amplitude of the differences due to nuclear motion is system-dependent. In BMA[5,5], electron dynamics seems to be too fast for the nuclear motion to have a significant effect. However, in BMA[6,5] and BMA[6,7], the effects are significant after only 5 fs. Nuclear motion can affect both the nature and timescale of charge migration. As expected, the interaction between electronic and nuclear degrees of freedom is stronger in molecular geometries where the electron dynamics slows down to the timescale of nuclear motion, i.e. where the energy gap is smaller.

Although the nuclei were moving in the above simulations, a single Ehrenfest trajectory was considered. To understand further the extent to which neglecting the nuclear wavepacket width is a reasonable approximation, we have used the Wigner distribution function (Wigner, 1932) – a quantum distribution function in classical phase space – to generate a set of geometries that represent the delocalized nuclear wavepacket and we have simulated electron dynamics at each of the geometries before averaging the properties over the ensemble. Figure 4a shows the electron dynamics in BMA[5,5] for an

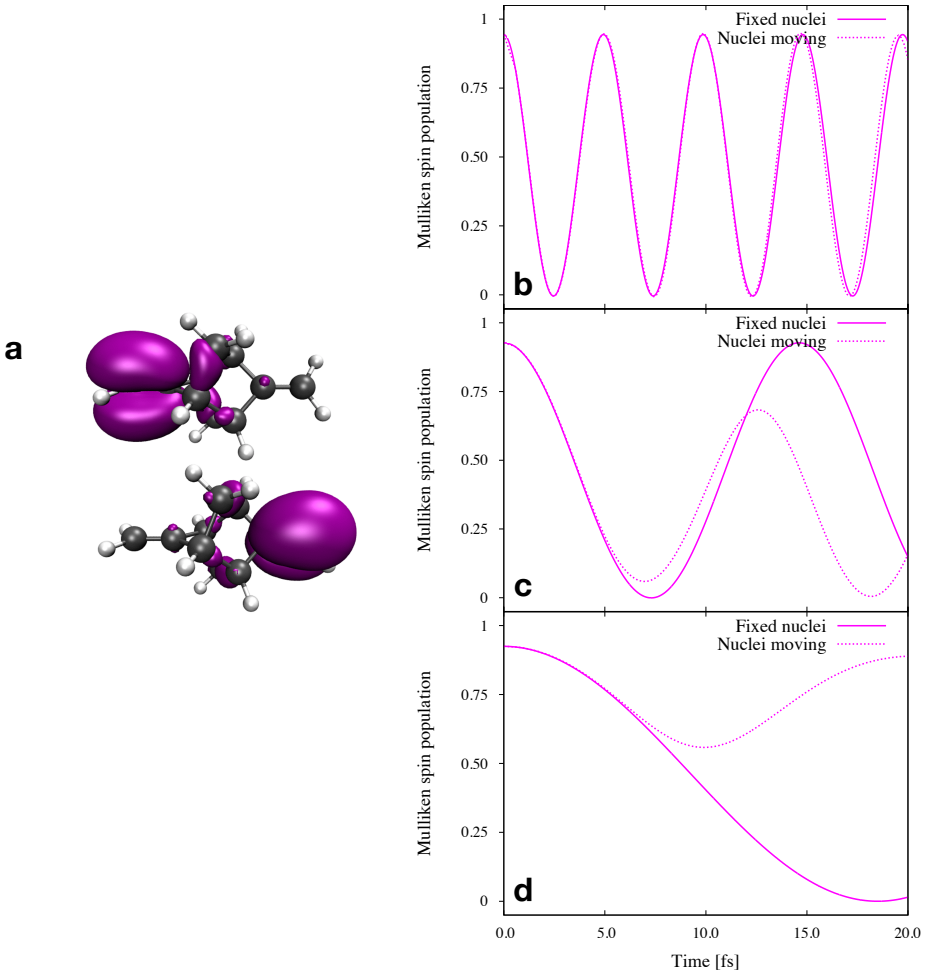

Figure 3: **a**: Modified bismethylene-adamantane molecule where the cage consists of four connected cyclopentane (instead of cyclohexane) rings (BMA[5,5]) and its time-dependent electronic spin density at the turning points of the oscillations (t = 0 and t = 2.4 fs). **b-c-d**: Time evolution of electronic spin density partitioned on the left methylene group in the BMA[5,5], BMA[6,5] and BMA[6,7] molecules, respectively, with fixed nuclei (solid lines) and nuclei moving classically according to the Ehrenfest method (dashed lines). Adapted from (Vacher et al., 2016a) with permission from the Royal Society of Chemistry.

ensemble of 500 nuclear geometries, simulated independently. A close look allows one to distinguish the individual oscillations with different periods (in purple). The average oscillation amplitude for the ensemble is shown as a solid/dashed white line for fixed/moving nuclei. We observe several oscillations, the amplitude of which is damped with time. We can extract a coherence half-life of ≈ 7-8 fs. In summary, the effect of the nuclear wavepacket width is extremely important (and can be larger than that of the nuclear motion *per se*): it leads to a fast dephasing of the electron dynamics. We have obtained similar results for other molecular systems (Vacher et al., 2015c; Jenkins et al., 2016a,b). We have also developed a simple analytical model to explain the molecular properties affecting the electronic coherence lifetime: namely, the width of the nuclear wavepacket and the relative slope of the involved potential energy surfaces (Vacher et al., 2015c).

In the previous simulations, the nuclei were treated classically and the nuclear trajectories were simulated independently. The Ehrenfest method may underestimate the effect of the nuclear motion on electron dynamics since it is a mean-field approach. Also, the use of independent simulations to represent the natural distribution of positions and velocities in the nuclear wavepacket may overestimate the dephasing of electron dynamics. To investigate to what extent the use of a fully quantum mechanical treatment is important, we have used the DD-vMCG method to simulate charge migration in BMA[5,5] coupled to quantum nuclear motion (Figure 4b) (Vacher et al., 2017). The 1-GBF simulation is equivalent to a single Ehrenfest trajectory. Convergence is reached when including 17 GBF. The more realistic description shows several oscillations, again damped with time. Electronic decoherence is confirmed with fully quantum nuclear dynamics, with a 6-fs coherence half-life. An in-depth analysis of the quantum dynamics simulations shows the interplay of different mechanisms. The non-adiabatic electronic relaxation has little effect on the coherence lifetime. The dephasing mechanism leads on its own to very fast decoherence (in agreement with the previous mixed quantum-classical results), while the total electronic decoherence can actually be slower: taking into account the nuclear overlap decay partially compensates for the very fast dephasing and gives rise to small coherence revivals.

3.3. Coherence versus entanglement

The process of photoionization is a perfect example of breakup of a quantum system into distinct sub-systems: the photoelectron moving away and

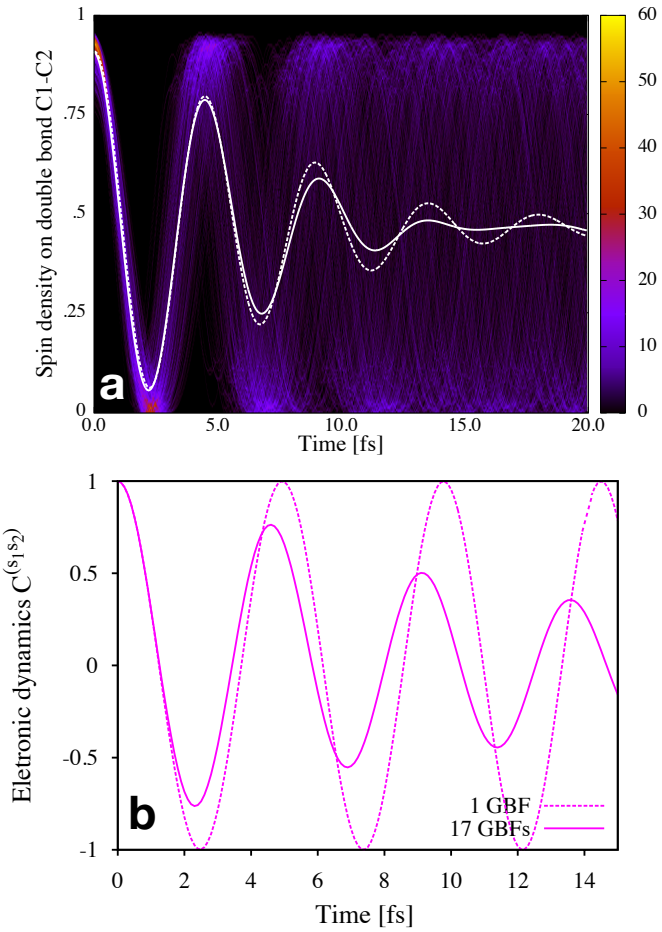

Figure 4: **a**: Time evolution of electronic spin density partitioned on the left methylene group in the BMA[5,5], with fixed nuclei (solid lines) and nuclei moving classically according to the Ehrenfest method (dashed lines), for an ensemble of 500 geometries initially sampled from a Wigner distribution. **b**: Same as **a** with nuclei moving quantum mechanically according to the DD-vMCG method. Adapted from (Vacher et al., 2016a) with permission from the Royal Society of Chemistry, and from (Vacher et al., 2017) with permission from the American Physical Society.

the parent ion that is left behind. In the case of atomic photoionization, the remaining parent ion can in general consist of a bound or highly-excited many-electron system, while in the molecular case additional breakup of the nuclear quantum system, such as fragmentation, can also be triggered during the process.

As a result, two interrelated, fundamental quantum-mechanical concepts characterize the many-body dynamics upon photoionization: quantum coherence and quantum entanglement. For example, quantum electronic coherence in photoionized molecules, arising at the attosecond and persisting at the femtosecond timescales, underpins the few-femtosecond charge dynamics and therefore also the ensuing photochemical transformation of matter.

From a quantum mechanical point of view, maximal quantum coherence within either the photoelectron or the parent ion sub-systems that are formed upon photoionization implies that, at large spatial separations between the two, the time-dependent, N-electron wavefunction of the total photoionized system $\Psi^N(\mathbf{x}_1, ..., \mathbf{x}_i, ..., \mathbf{x}_N; R, t)$ is separable in the degrees of freedom of the two formed sub-systems. Note that here the parameter R stands for the nuclear coordinates, which can also become a dynamical variable, on equal footing with $\mathbf{x}_i$, when nuclear dynamics effects are important. Thus, the wavefunction of the composite N-electron system can be written, at least to a good approximation, as the (anti-symmetrized) product of a $(N-1)$-electron wavefunction (in principle fully correlated) describing the parent ion, i.e. only dependent on ionic degrees of freedom, and a one-electron wavefunction describing the photoelectron

$$\Psi^N(\mathbf{x}_1, .., \mathbf{x}_i, .., \mathbf{x}_N; R, t) \approx \hat{A}\left[\Psi^{N-1}(\mathbf{x}_1, .., \mathbf{x}_i, .., \mathbf{x}_{N-1}; R, t) \times \psi^{e^-}(\mathbf{x}_N; t)\right]. \tag{38}$$

The product Ansatz of Eq. (38) is valid only when quantum coherence is at maximum within each sub-system, which can be consequently described itself as a pure state, i.e. with a well-defined wavefunction.

In the more general case, the total bipartite system is described by a time-dependent density matrix $\hat{\rho}(t)$. As already discussed in sub-section 3.1, each of the separate sub-systems is itself described by a reduced density matrix that is obtained by tracing out the extra degrees of freedom pertaining to the other, unobserved, sub-system. The partial trace operation gives rise in general to a mixed quantum state for the resulting sub-system. This is the case even when the total density matrix $\hat{\rho}(t)$ corresponds to a pure state,

i.e. $\hat{\rho}(t) = |\Psi^N\rangle\langle\Psi^N|$. Spectral decomposition of, for example, the R-IDM

$$\hat{\rho}^{R-IDM}(t) = \sum_I r_I(t) \; |\tilde{\Psi}_I^{N-1}(t)\rangle\langle\tilde{\Psi}_I^{N-1}(t)|, \tag{39}$$

allows one to express the mixed quantum state of the parent ion system, at each time t, as a statistical ensemble of orthogonal pure quantum states, each populated with weight (probability) $r_I(t)$ and with the correspondent projection operator given by $|\tilde{\Psi}_I^{N-1}(t)\rangle\langle\tilde{\Psi}_I^{N-1}(t)|$. This is a very different situation with respect to the one described by Eq. (38), where there was a single, well-defined wavefunction $\Psi^{N-1}(\mathbf{x}_1,..,\mathbf{x}_i,..,\mathbf{x}_{N-1};R,t)$ representing the parent ion. The global quantum coherence of the mixed quantum state of the ionic system can be quantified by the so-called ionic purity

$$p(t) = Tr\left[\hat{\rho}^{R-IDM}(t) \times \hat{\rho}^{R-IDM}(t)\right], \tag{40}$$

$$0 \leq p(t) \leq 1,$$

which is a "global" quantity, i.e. independent of the specific basis set used.

So far we have only discussed quantum coherence. Let's now turn our attention to the entanglement between the two sub-systems. The state of Eq. 38 describes a physical scenario in which the photoelectron and the parent ion systems are not entangled with each other. In order to obtain an entangled state, we can modify Eq. 38 as follows

$$\begin{aligned}\Psi^N(\mathbf{x}_1,..,\mathbf{x}_i,..,\mathbf{x}_N;R,t) &\approx \sum_K C_K(t) \; \hat{A}\left[\Psi_K^{N-1}(\mathbf{x}_1,..,\mathbf{x}_i,..,\mathbf{x}_{N-1};R) \times \psi_K^{e^-}(\mathbf{x}_N)\right] \\ &\approx C_1(t) \; \hat{A}\left[\Psi_1^{N-1}(\mathbf{x}_1,..,\mathbf{x}_i,..,\mathbf{x}_{N-1};R) \times \psi_1^{e^-}(\mathbf{x}_N)\right] + \\ &+ C_2(t) \; \hat{A}\left[\Psi_2^{N-1}(\mathbf{x}_1,..,\mathbf{x}_i,..,\mathbf{x}_{N-1};R) \times \psi_2^{e^-}(\mathbf{x}_N)\right] + ...\end{aligned} \tag{41}$$

Here, $[\Psi_K^{N-1}]$ and $[\psi_K^{e^-}]$ are two linearly-independent set of wavefunctions for the parent ion and the photoelectron sub-systems, respectively. The state of Eq. 41 reduces to the one of Eq. 38 when only one C_K coefficient is non-null, while it is non-separable as long as at least two time-dependent coefficients C_K are different from zero. A possible, basis set independent, measure of the entanglement between the parent ion and the photoelectron is given by the *von Neumann entropy of entanglement* $s(t) = -\sum_I r_I(t) \times \ln(r_I(t))$. The more entangled the two sub-systems are, the more mixed (i.e. with less quantum coherence) the state of each of them is. This can already be inferred by observing that eq. (41) does not offer a uniquely,

well-defined wavefunction for the parent ion. It can also be easily seen by comparing eq. (38) and eq. (39): maximal coherence requires the parent ion to be described by a pure state, i.e. by a well-defined $(N-1)$-electron wavefunction, which can be expressed in any arbitrary basis as a specific *fully coherent* linear superposition of the basis states. Therefore, the spectral decomposition of eq. (39) must only have one r_i term different from zero (and consequently equal to 1). This requirement automatically gives us a minimum value for the entropy of entanglement, equal to 0, and a maximum value for the purity, equal to 1.

This inherent relationship between coherence and entanglement can be also observed in Figure 5, where we show the time evolution, following XUV ionization of the pyrazine molecule, of the ionic purity and the *von Neumann entropy of entanglement* between the parent ion and the photoelectron (Ruberti, 2021). During the process in which the photoelectron is leaving the parent ion, the residual interaction between the two sub-systems increases their entanglement, which is indeed accompanied by an overall decrease of the quantum coherence within the parent ion.

The entanglement we have discussed thus far is the one which is created by the photoionization process between the photoelectron and parent ion. This type of entanglement can be encoded in the different degrees of freedom of the two sub-systems. For example, in the case of the parent ion, it can either be imprinted in its electronic or in its nuclear (e.g. vibrational) degrees of freedom. A nice example of entanglement upon photoionization between the vibrational states of the parent ion and the kinetic energy states of the photoelectron is illustrated in (Vrakking, 2021; Koll et al., 2022), where the photoionization of the H_2 molecule by a pair of time-delayed attosecond XUV laser pulses is considered within a simplified model. The inherent relationship between coherence and entanglement detailed above is also discussed in (Vrakking, 2021; Koll et al., 2022), where it is shown how an increase (or decrease) of the entanglement between the photoelectron and the parent ion leads to a decrease (or increase) of the degree of vibrational coherence in the latter system and how to control these quantities by tailoring the spectral properties of the photoionizing pulses.

Finally we would like to remark that even when the parent ion system is fully coherent, i.e. described by a pure state, entanglement can still exist between its internal (nuclear and electronic) degrees of freedom. The time evolution of this entanglement, which is driven by the interactions between the electron and the nuclei, can in principle lead to the decoherence of the

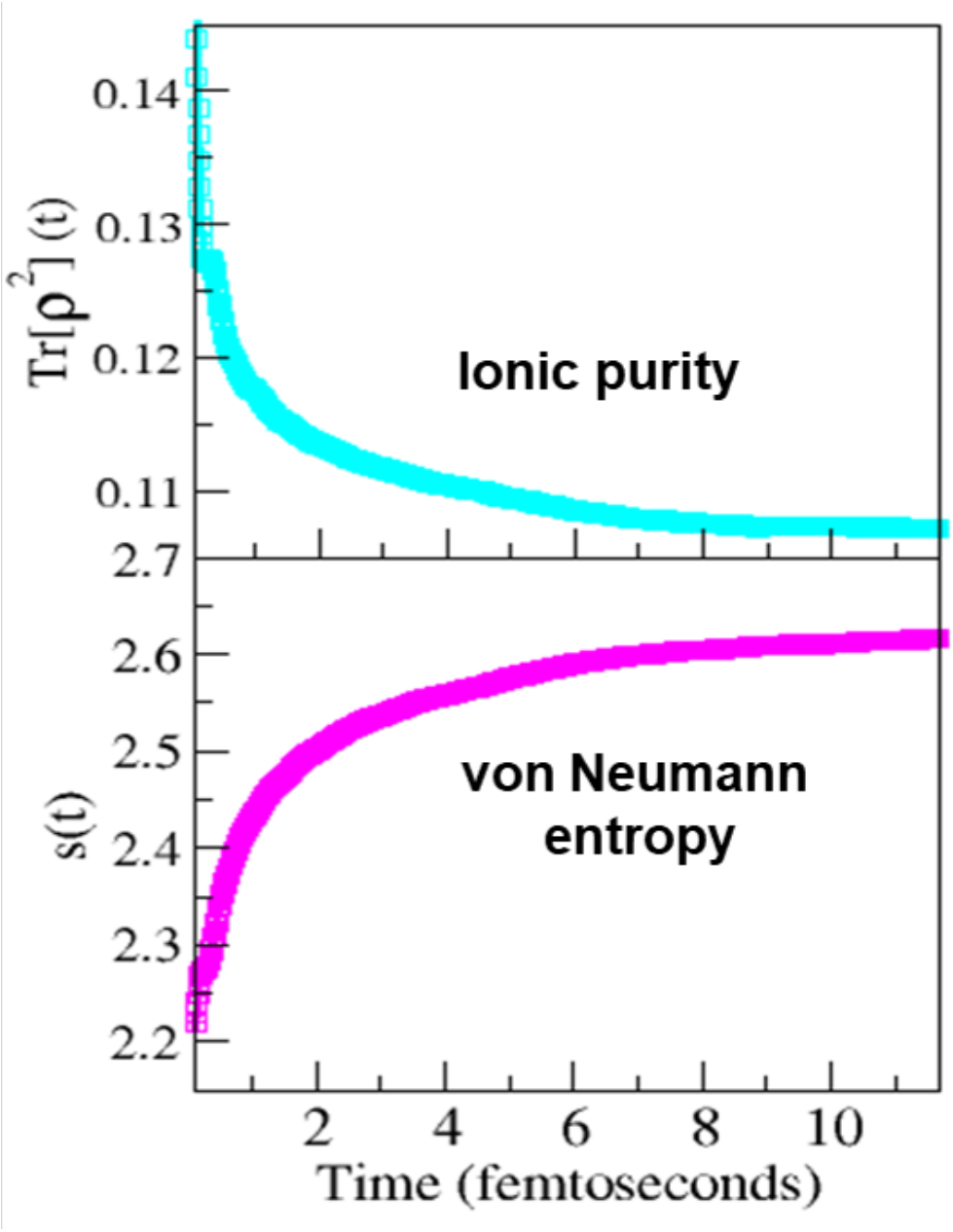

Figure 5: Time evolution of the ionic purity $Tr[\rho^2](t)$ (upper panel) and the *von Neumann entropy of entanglement* s(t) (lower panel) between the parent ion and the photoelectron after XUV ionization of the pyrazine molecule. Adapted from Ref. (Ruberti, 2021) with permission from the Royal Society of Chemistry.

many-electron sub-system and potentially also to situations where its coherence can exhibit revival structures, as discussed previously in subsection 3.2.

4. Observations of attosecond molecular dynamics

4.1. Pump-probe methodology for tracking electronic coherence

As is generally the case for measuring ultrafast dynamics a pump-probe methodology can be applied to follow attosecond timescale dynamics. Some special features of the methodology must be included to ensure that the full electronic wavepacket dynamics can be accessed. For the electronic wavepacket to be measured in an experiment, it is necessary that the states within that wavepacket are projected onto the same final state(s). Then the interference due to the relative phases and amplitudes of states in the superposition can be read out. The sequence for measurement of attosecond charge dynamics is therefore as follows: (i) an initial event impulsively (within the sudden approximation) initialises an electronic wavepacket (ii) which then evolves for some time, τ; (iii) and a second event drives a transition to a final state or states, (iv) and then the population in the final state is measured. The population of the final states can be used to infer the phase and amplitude of the states within the wavepacket after its evolution for the period τ. The experimentalist seeks to control steps (i), the pump, and (iii), the probe, whilst choosing an appropriate method for (iv), the measurement. Step (ii) can also be controlled, which is the aim of quantum control. In nature the manifestation of the wavepacket dynamics is also through some potential observable, such as the evolution of the position expectation value that results in an oscillatory charge density which can couple to the vibronic modes of the molecule.

The experimental measurement of attosecond timescale dynamics has only been possible in the last few decades. Methodologies such as core-hole clock spectroscopy (Wurth and Menzel, 2000), relying on internal ultrafast dynamics within the quantum system under consideration to time events, had been applied previously. Nevertheless, it has only been with the emergence of attosecond technology over the past 20 years that sub-femtosecond duration pulses of light (extreme UV to x-ray) have become available and through these it has become possible to make measurements of general time domain processes in this temporal regime. Two broad classes of sources of attosecond pulses exist relying either on high order harmonic generation from

ultrashort optical pulses or generation of very short x-ray pulses using an appropriately configured x-ray free electron laser (XFEL).

4.2. High harmonic generation based attosecond measurements

The first method to emerge as a source of attosecond light pulses was high order harmonic generation (HHG), and this has, up until now, driven most research in the area. Two methodologies of using HHG to measure molecular attosecond dynamics have been developed: (a) $in-situ$ methods such as high-harmonic generation spectroscopy, where the ionisation of the medium to be studied initiates the dynamics and the harmonic emission from the molecule carries the signatures of the attosecond dynamics; (b) $ex-situ$ measurements where HHG carried out in one location is used to generate an isolated attosecond pulse, or an attosecond pulse train, and this is delivered to a second location where it is used as either the pump or probe in a measurement on the system of interest. We will discuss the HHG spectroscopy methods below (case study 3) in the context of the first experiments that used this to study fast nuclear (proton) dynamics in H_2 and CH_4 (Baker et al., 2006) as well as a more recent example. We will explain that a major disadvantage of this methodology is that the measurement is always performed in the presence of a strong (10^{14} W·cm^{-2}) optical field that may seriously perturb the dynamics to be studied.

The $ex-situ$ pump-probe methods have been developed in a number of forms. If a photoelectron or an Auger electron emission is to be measured the temporal/phase properties of that process can be followed using the attosecond streaking method, if an isolated attosecond pulse is used (Drescher et al., 2002), or an interferometric (RABBIT) methodology if using a pulse train Paul et al. (2001). These methods have been demonstrated to be powerful for studying photoionisation dynamics of atoms, molecules and even surfaces. They do not, however, shed much light on the internal evolution of the molecule following ionisation unless that dynamics are also accompanied by an Auger emission. In many cases the key feature of the cation is an electron-hole in the valence states (or superposition of those states) that is energetically forbidden to Auger decay, as is the situation in the most widely discussed examples of *charge migration*. Tools to study this using a short optical pulse to induce further molecular fragmentation have been applied to the case where the cation was excited by an attosecond XUV pulse Calegari et al. (2014). These studies may also be hampered by the strong field and the limited temporal duration of the optical probe pulses (typically > 3 fs).

Avoidance of the distortion due to the strong optical field and improved temporal resolution is being tackled by the development of few-femtosecond UV and deep UV pulses and the application of a second XUV attosecond pulse.

4.3. Time-resolved x-ray spectroscopy and photoelectron spectroscopy

Transient x-ray absorption spectroscopy (XAS) provides an alternative to fragmentation studies, and offer a more direct measurement of the evolution of the charge wavepacket through targeting the electronic observables of the system. The absorption is generally characterized in relation to the atomic edges where the absorption is spectrally located, i.e. the K- or L-edge (arising from the n=1 and n=2 shell core states to continuum transitions), and sometimes the M-edge (arising from the n=3 shell).

Absorption just below these edges is due to transitions from core to unoccupied valence states including valence hole states. A photon can be absorbed when a few conditions are met: it is resonant between the core state and a valence state, the core state is populated, the valence state is unoccupied or only partially occupied, and there is a non-zero transition matrix element. In practice, the last condition is a requirement on the symmetry of the molecules that they satisfy the dipole selection rules. With high resolution measurements the different transitions are visible as separate Lorentzian absorption peaks. Absorption in this pre-edge region therefore directly probes the populations of valence states and valence electron holes, with the positions of the peaks giving information on the chemical environment local to the atomic site being probed.

XAS in the near-edge region acts as a probe of the electronic coherences by projecting the wavefunction of the molecule onto a core excited state. Specifically, cross-sections for transitions are proportionate to the projection of the molecular wavefunction $\Phi_i(\tau)$ onto a final state Φ_f via the total electron momentum operator,

$$\sigma_{\mathrm{XAS}}(\tau) \propto \left|\langle \Phi_f | \, \mathbf{p} \, | \Phi_i(\tau) \rangle\right|^2 \rho_f(E), \tag{42}$$

where $\rho_f(E)$ is the density of states at the energy of the excitation. The extent at time τ of valence hole localisation close to a specific atomic centre, associated with the core-excited state, is a sensitive and direct measure of the wavepacket dynamics using time-resolved XAS probing. Due to the temporal width of the probe the time-delay of the measurement is smeared out and the measured cross-section is convolved with the envelope of the

attosecond pulse. The measurement can be directly of the absorption, by measuring the attenuation of the x-rays. In krypton, for example, the coherence of three valence excited states in an electronic wavepacket excited by strong field ionisation was measured by XAS, lasting for 10s of femtoseconds (Goulielmakis et al., 2010). It can also be indirect, measuring either photoemission or autoionisation (Auger electrons) following the decay of the core-excited state.

Photoelectron spectroscopy (PES) using HHG and XFEL sources has been widely applied to the study of ultrafast phenomena, in both gas and condensed phase systems. However, for the study of attosecond dynamics, the challenge of the time-bandwidth limit requires customised source spectral filtering of an otherwise very broad bandwidth HHG derived sources to provide finite enery resolution, although recent work with XFELs where the intrinsic time-bandwidth product (0.5 fs/2 eV) has proven more amenable to such studies. Core electrons are sensitive to their chemical environment and may provide a route to probing local charge density (Gelius and Siegbahn, 1972), and further work in this area seems likely. XFELs are well placed for these time-resolved x-ray photoelectron spectroscopy (XPS) measurements (see below).

For the *ex-situ* methods where the HHG emission is used as a probe, a pump of sufficiently short duration is also required, which either excites the neutral molecules or photo-ionises them to form cations. For excitation of neutral molecules by a single-photon excitiation, conservation of energy requires that the coherent bandwidth in the pump pulse must span the energies of transitions from the electronic ground state to each state within the wavepacket. This is possible with femtosecond timescale pulses for charge dynamics involving only couplings of isolated valence and has been demonstrated in, for example, the ring opening of 1,3-cyclohexadiene, but for the few-femtosecond or attosecond dynamics involving coupling to multiple valence states, a few eV bandwidth is typically required (Attar et al., 2017). This is currently a challenge in all optical set-ups and effort is underway to find options which are also capable of creating excitation fractions high enough for measurement. With advances in HHG sources in the form of improved focusing to overcome the low pulse energy (typically $< 10^6$ photons per-pulse on target) and higher repetition rate lasers (10 - 100 kHz) the prospects for attosecond XUV-XUV pump-probe measurements look promising (Kretschmar et al., 2022). Femtosecond UV sources based on dispersive wave formation in gas filled fibres may also meet this requirement (Travers

et al., 2019), and combining such sources with HHG pulses in a pump-probe configuration is being actively pursued.

4.4. Strong field pumps and probes

Strong field ionisation can create a wavepacket without the same bandwidth requirements on the pulse-envelope needed for single-photon ionisation as the ionisation occurs on a timescale much shorter than an optical cycle. Strong field ionisation occurs when the electric field is sufficiently strong for electrons to tunnel into the continuum or, for even stronger fields, to ionise over the Coulomb barrier. The most readily available sources for strong field ionisation are infrared pulses. Further temporal confinement, to an ionisation event within a single half-optical cycle, is being sought using the methods of self phase modulation either in gas filled hollow core fibres (Nisoli et al., 1996) or filaments (Stibenz et al., 2006) to generate octave spanning IR sources which can be compressed to a single half-cycles. However, at the time of ionisation, the molecule is in the presence of a strong field. At least for the early stage of its evolution, the wavepacket is therefore also in the presence of a strong field, which will alter the dynamics (Lezius et al., 2002; Guo et al., 1999). Furthermore, interaction with the ionised electron, which is also evolving under the presence of a strong field, cannot be ignored. Therefore, to model these measurements the strong field must be accounted for in the dynamics. Even if this is computationally feasible, it is then difficult to interpret results and apply them to photochemical dynamics, which are typically free of strong fields.

Alternatively, *ex-situ* measurements can use the XUV/soft x-rays as a pump. The probe will still ionise, but as this is a single photon process the electric field can be low enough so as to have a negligible effect on the evolving wavepacket. With valence ionisation using an x-ray (> 100 eV pump) the sudden approximation is rigorously applicable. For HHG based VUV (10 to 20 eV) pump sources, however, this breaks down although HHG sources in this energy range give orders of magnitude higher excitation fractions due to increased fluence and higher cross-sections compared to the x-ray range. The difficulty is then in finding a suitable probe of the electron wavepacket, and present laser technologies again lead to the use of strong field ionisation. A strong field probe can either interact with the electrons bound to the molecule, causing tunnel ionisation, or with ionised electrons in a process referred to as attosecond streaking. The rates of tunnel ionisation depend on the electronic wavefunction. Consequently, the final charge state of the

molecule provides an indirect measure of the wavefunction. Typically, this can be obtained by measurement of ion yields. Furthermore, these doubly ionised molecules will generally fragment, with the fragment yields depending on the charge density distribution at the time of ionisation. In xenon ions, it was first demonstrated that this technique is capable of time resolution below a half-cycle of the probe (Uiberacker et al., 2007).

Molecules have become accessible to these methods in the past 8 years, beginning with the landmark measurement of ion fragments following ionisation of phenylalanine with isolated attosecond VUV pulses from an HHG source Calegari et al. (2014). Approximately 4.3 fs oscillations on top of a longer, 25 fs decay, were attributed to a coherence superposition of 1h cationic states. Subsequent experiments in a larger molecule, the amino acid tryptophan, explored the role of nuclear dynamics. There the Ehrenfest method was employed in the interpretation. They found, using a single Ehrenfest trajectory and thus neglecting zero-point energy nuclear wavepacket spreading, that coherent charge dynamics can still occur over 10s of femtoseconds, despite nuclear motion (Lara-Astiaso et al., 2018). A recent experiment using a similar methodology looked at doubly charged fragments from strong field ionised adenine as a signature of shake-up excitations of ionised adenine following ionisation, which drive out-of-plane charge migration (Månsson et al., 2021). In our first case study on the molecular cation of isopropanol (subsection 5.1), we discuss an experiment using isolated attosecond pulses from an HHG source, where ion fragments are used as a signature of nuclear motion in conjunction with an all x-ray pump-probe absorption measurement of the dynamics resulting from correlations with 2h-1p states in isopropanol molecules.

4.5. XFEL based few-femtosecond to attosecond domain measurements

X-ray free electron lasers (XFELs) offer an alternative, and powerful, source of short x-ray pulses for probing attosecond dynamics. In an XFEL undulator, self amplified spontaneous emission (SASE) in the high gain regime will select a single transverse mode from an initially noisy distribution (Kim, 1986), and therefore result in good spatial coherence. However, temporal coherence is less assured and is determined by the coherence length of the electron bunch (Kim et al., 2017). To a good approximation, within each coherence length of the electron bunch, a single SASE spike is emitted. Therefore the ratio of the electron bunch length and the coherence length gives the total number of SASE spikes, which can be up to a few hundred emission

spikes in each pulse. A second implication of this is that the overall temporal length of SASE pulses is limited by the length of the electron bunch. Methods for creating shorter pulses in general seek to compress the bunch, or restrict the lasing to a small portion of it to limit the x-ray emission to a single SASE spike. For example, an early successful method for producing pulses of controllable temporal duration, down to 8 fs was the insertion of a slotted foil into the centre of a chicane bunch compressor (Emma et al., 2004). When the bunch passes through the foil, all but a small section of the bunch is Coulomb scattered and the emittance 'spoiled', reducing the effective length of the electron bunch that can lase.

XFELs can be used for the same *ex-situ* measurements as HHG sources when synchronised to an external laser field (Erk et al., 2014). However, it is not currently possible to synchronise to better than 10 fs and drifts have been reported on the order of 100's of picoseconds. The best that can be achieved is by measuring the delay on each shot and sorting by time delay afterwards, but this is still limited to several femtoseconds (Harmand et al., 2013). What XFELs do however offer, is the possibility for all x-ray measurements by generating two pulses from one electron bunch, giving site specificity to both the pump and probe (Picón et al., 2016) for angstrom spatial and attosecond temporal resolutions. An early all x-ray measurement using 10 fs pulses was able to study proton transfer in acetylene at the limit of the measurement resolution (Liekhus-Schmaltz et al., 2015) and fragmentation of buckminsterfullerene was measured with 20 fs resolution Berrah et al. (2019).

The state-of-the-art for creating short pulses relies on enhanced SASE (eSASE), already treated theoretically in 2005 (Zholents, 2005), and recently implemented (Duris et al., 2020). The principal components of eSASE are an infrared beam overlapping longitudinally with the electron beam in a wiggler section and a following chicane. In this case the source of the infrared beam is emission from the electron bunch within the wiggler. This generates broadband low frequency radiation, which avoids the difficulties involved with synchronising the electron bunches with an external laser. The infrared beam imparts a sinusoidal energy modulation on the electron bunch's spatial distribution. The chicane is dispersive, i.e. low energy electrons follow a longer path and high energy electrons follow a short path, thus mapping the energy distribution of the bunch into space, with sharp temporal localisation of the high electron density at each zero of the sinusoid. Using this technique, pulses shorter than 500 as FWHM have been been generated and measured

using angular streaking (Duris et al., 2020). In contrast to HHG sources, XFELs produce large numbers of photons in a single pulse, for example, 100 uJ at the 500 eV corresponds to 10^{12} photons. Attosecond XFELs are also the ideal x-ray sources for investigation of nonlinear x-ray processes O'Neal et al. (2020).

5. Case studies

In the first two case studies, we discuss two recent experiments in which we have extended the XFEL methods to the study of charge migration, for the first time. Work is now progressing to use the attosecond XLEAP capability for pump-probe measurements of charge migration. These measurements have used both time-resolved XAS and XPS methodologies and strong signatures of charge migration with sub-femtosecond resolution has been found. This technique looks set to make an impact on the study of charge migration and ultrafast electron-nuclear coupling in molecules in both gas and condensed phase over the next few years. This will be discussed further in Section 6.

5.1. Transient XAS in isopropanol

The first experiments we would like to discuss probed the rapid hole migration in isopropanol following ionisation Barillot et al. (2021). Two experiments on isopopropanol cation dynamics were separately performed, both in pump-probe configurations. The dynamics that we wished to probe in these experiments were those which followed the impulsive excitation of an inner valence hole, i.e. a hole insufficiently energetic to Auger-Meitner ionise, but where the breakdown of the molecular orbital picture of ionisation leads to a superposition of states capable of attosecond dynamics.

The first experiment used isolated attosecond pulses from an HHG source to initiate the hole dynamics and strong field IR pulses to further ionise, whilst measuring ion fragments. Figure 6a shows the delay dependent yield of high kinetic energy CH_3^+, which is sensitive to the length of the carbon-carbon bond. This probes the electronic excitations only through their coupling to the nuclear degrees of freedom.

In contrast, the second measurement, which used a two-colour mode of an XFEL for both pulses, was able to probe more directly the hole populations. The pump step of the experiment involved single x-ray photon excitation of an inner valence hole (IVH), and the IVH state time-dependence was probed

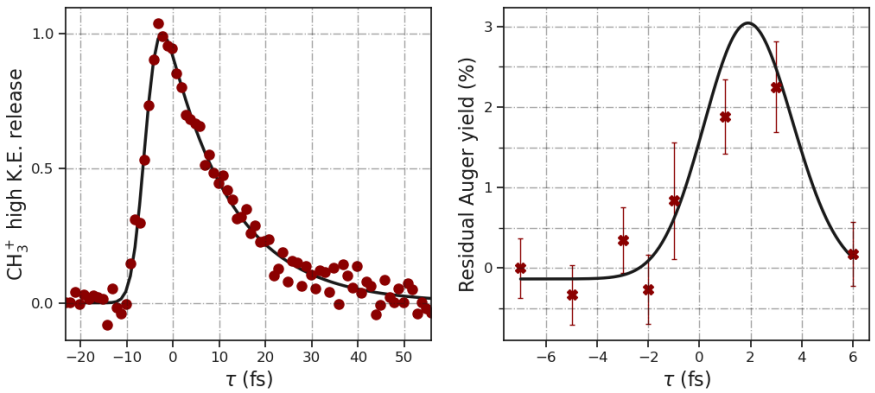

Figure 6: (a) Using a pump at 20 eV of 600 attosecond duration and a 4 fs IR probe, to induce transitions to the second ionization continuum, isopropanol cation dynamics was studied. Transient high kinetic energy CH3+ ion yield, attributed to the decay of the intermediate cationic channel in isopropanol, are observed with a decay time of 13 fs indicating nuclear dynamics on this timescale in the cation. (b) XAS measurement of a cationic hole state formed in isopropanol (see Figure 7) with an x-ray pulse and probed resonantly via a transition from the O 1s state to the inner valence hole vacancy corresponding to the 6a state. The signal is registered by measuring the delay dependence of the resulting Auger-Meitner electrons. This resonance, which maps the 6a hole population, reveals a highly transient hole state with the measured lifetime, limited by the instrument response function, of 1 ± 2 fs which is consistent with the correlation driven charge migration predicted by ADC theory.

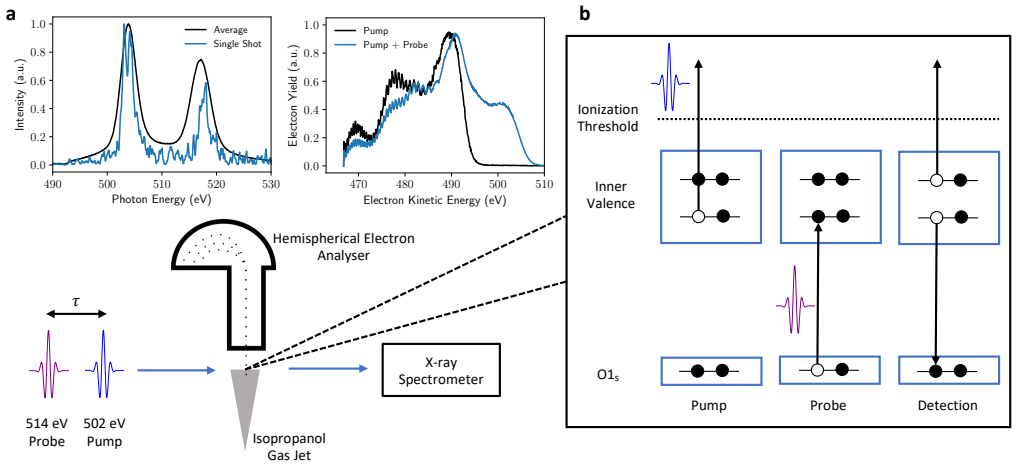

Figure 7: (a) For the XAS measurement two colour pulses (pump central photon 502 eV, probe central photon energy 514 eV) from the LCLS XFEL, with a chicane controlled delay, are directed to the isopropanol sample at the interaction point of a hemispherical electron analyzer. A down-stream x-ray spectrometer is used to determine the pulse spectra and relative energies on every shot. (b) The measurement process is summarised: pump step opens a number of valence ionization channels including creation of inner valence holes (IVH). The delayed probe pulse can strongly interact via a O 1a–IVH transition (a channel only open if inner valence ionization of the specific state has occurred). Following this there can be Auger-Meitner decay back to the O 1a hole with the emission of Auger-Meitner electrons of characteristic energy that can be detected. Adapted from (Barillot et al., 2021) with permission from the American Physical society.

through resonant absorption from the O 1s state at the oxygen site, which can be observed through subsequent Auger decay as proposed by Cooper et al. (2014). An experimental overview is shown in Figure 7. The pump and probe were tuned to 35 eV and 20 eV below the oxygen K-edge, but with spectral jitter of 5 eV, allowing the pulses to sample a range of energies. When the probe was on resonance, and following valence ionisation from an inner valence state, a transition from the oxygen K shell (1s) to the inner valence hole was possible, as shown in Figure 7c.

Figure 6b shows the time dependent Auger yield in resonance with the 6A hole, which lies just above the double ionisation potential. A short-lived transient hole state with a response limited 1^{+2}_{-1} fs lifetime is observed. The timescale of this measurement, an order of magnitude faster than nuclear dynamics, suggests purely electron correlation driven charge motion, i.e. charge migration. In this case it takes the form of a breathing mode of

the electron hole, that is initially localised near the oxygen site and then distributes over more spatially delocalised states before in principle moving back to the oxygen site. However, in comparison to the ab intio calculations, the dynamics are shorter-lived and lack revivals coherent revivals of the IVH population. Ab intio calculations of molecules at the equilibrium geometry, and with frozen nuclear motion predict significant population surviving for 10s of femtoseconds. The rapid decay of this transient could only be explained by using calculations of the hole lifetimes which include relevant zero-point energy spreading of the initial nuclear geometries. The result is that the zero-point geometry spread masks longer lived oscillatory dynamics due to a phase spread between the revivals of different geometries. These two measurements highlight the importance of nuclear dynamics in what is often described as 'purely electronic' motion. Motion of even the C-C bonds is significant on the 10 femtosecond timescale (C-H bond motion is faster) and the spread in the initial geometries dominates in the first few femtoseconds. Even for isopropanol, a small molecule, this poses a significant challenge to theory.

5.2. Electron-nuclear coupling in glycine

The example discussed above of the observation of a transient hole in the Auger forbidden energy region involved essentially a single breathing motion of the electronic wavepacket without subsequent oscillations. More recently carrying out similar experiments in glycine a true oscillatory electronic wavepacket motion has been seen using time resolved XAS (Schwickert et al., 2022).

In this work observation of oscillatory hole motion using XAS tuned to 272 eV, i.e. just below the C K edge, was employed as the primary method. Here the FLASH free electron laser in Hamburg was used to produced single-SASE spike pulses at this photon energy with a pulse duration of < 3 fs. Each pulse was split using a split-and-delay unit, comprising an actuated interleaved mirror to provide sub-femtosecond delay resolution, with the inter-pulse delay scanned from 0 to 175 fs. The glycine was introduced into the x-ray focus using a custom capillary delivery system that provided a sufficiently high local density of glycine vapour with negligible background gas. The electrons from photoelectron emission due to the pump step and the probe step that yielded C Auger electrons were measured using an electron magnetic bottle spectrometer. Coincidence between photoelectrons corresponding to ionisation from the target inner valence state in glycine ($10A'$) and the Auger

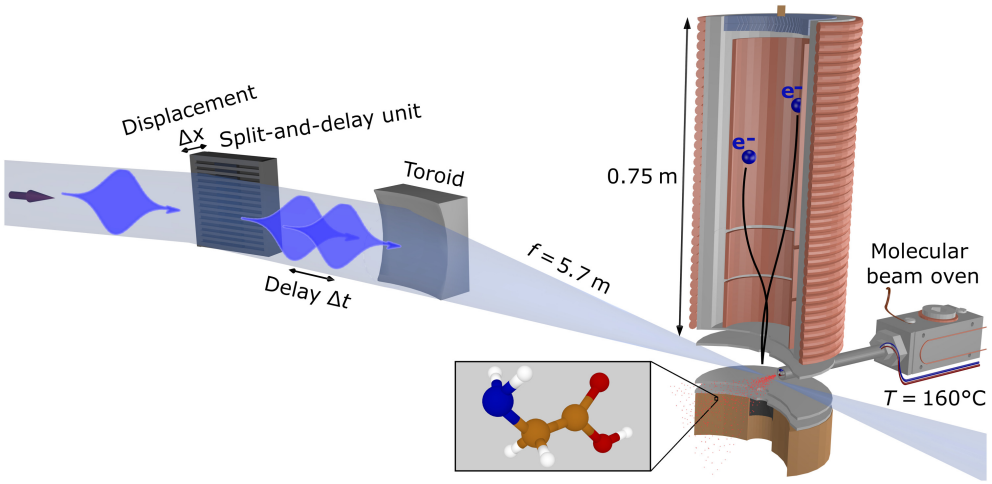

Figure 8: Experimental setup for the femtosecond x-ray pump-probe XAS measurements of inner valence hole states in glycine. The x-ray pulses from FLASH2 were of ~3 fs duration, tuned close to resonance at 276 eV, and delayed using a split-and-delay mirror system. The resulting Auger-Meitner electrons from the probe were detected in coincidence with the energy selected pump induced photoelectrons corresponding to the target state. Adapted from (Schwickert et al., 2022) with permission from AAAS.

electron channel was used to unambiguously identify the XAS probe signal.

The main result of these measurements was the observation at early times (delays less than 50 fs) of an oscillatory period of 19 fs in close agreement with the calculations of the $10A'$ state using B spline ADC that were used to compute the ionisation process and subsequent hole dynamics (see section 3). But at later times, i.e. for delays longer than 50 fs, the periodicity changes to closer to 30 fs as can clearly be seen in the lower panel of the figure that shows a windowed Fourier transform of the time-dependent signal trace (upper panel). These longer period oscillations have been attributed to the coupling of the initial purely electronic modes to modes of a mixed vibration-electronic character. Further theoretical work that now couples the high level electronic calculations to a full quantum treatment of the nuclear modes will hopefully more fully explain this critical observation of the electron-nuclear coupling, which is of high importance to our understanding of attochemistry.

5.3. HHG spectroscopy in deutriated and protonated molecules

The high temporal resolution available in the HHG spectroscopy technique arises from the intrinsic chirp of the recolliding electron wavepacket

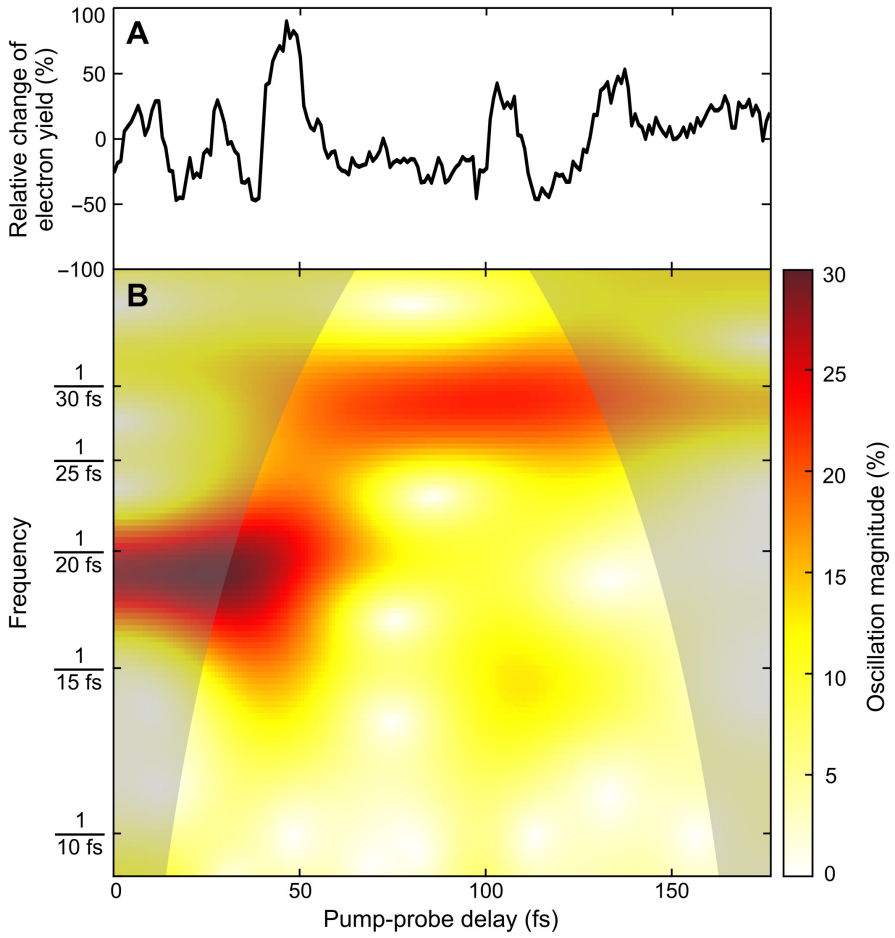

Figure 9: (a) Oscillations in the magnitude of the XAS signal induced and monitored with 272.7 eV photons. Relative change of the detected electron yield is correlated with both the generation of a Gly2+ parent ion and with an electron at the kinetic energy corresponding to valence ionization of 10A′ as a function of x-ray pump-probe delay in 1 fs steps (black line). (b) The continuous wavelet transform monitors the magnitude evolution of the non-stationary signal frequencies (false colour plot). The "cone of influence," where part of the wavelet in time domain extends past the finite recorded experimental signal trace, is given as a darker shaded area. Two dominant time periods of T = $19.6^{+1.5}_{-1.4}$ fs (over the first 40 fs) and T = $29.3^{+2.2}_{-2.0}$ fs (later on) can be extracted, with the initial period being in excellent agreement with the ab initio theory explaining the oscillations as a result of electronic coherence averaged over the nuclear geometries. The longer period observed after 40 fs is consistent with the excitation of vibronic modes in the molecular cation. Adapted from (Schwickert et al., 2022) with permission from the AAAS.

Baker et al. (2006). Electrons born into the continuum shortly after the laser field maximum of a particular optical cycle follow so-called *short trajectories* that return to the parent ion within an optical cycle. Each of these short trajectories, however, returns to the parent ion at a different delay time depending on the precise ionisation time, and each is associated with a different electron kinetic energy gained from the laser field at the point of recollision. This temporal spread leads to a frequency-chirped harmonic emission, with successively higher harmonics being generated at longer time delays. This attochirp has been measured previously by Mairesse et al. (2003). This property of HHG was used in studying very rapid proton dynamics in small molecules since it allows a range of pump-probe delays to be accessed by analysis of a harmonic spectrum with the intrinsic time to energy mapping encoded within it.

In these experiments it was necessary to compare the harmonic spectrum under identical conditions between protonated and deuterated isomers of the molecule. The ratio of the harmonic intensity between deuterated and protonated samples for different harmonic orders (photon energies) along with a knowledge of the chirp were used to retrieve the nuclear dynamics with a sub-femtosecond precision. We compared our experimental results with a calculation based on the strong-field approximation, which collected the effect of the nuclear motion in the compact nuclear correlation function. The harmonics are approximately proportional to the squared modulus of the nuclear autocorrelation function, $c(t) = \int \chi(R,0)\chi(R,\tau)dR$, where $\chi(R,0)$ and $\chi(R,\tau)$ are the initial and propagated vibrational wavepackets in the molecular ion, R is the internuclear distance, and τ is the electron travel time (or pump-probe delay). A retrieval of the dynamics was thus possible: it allowed insight into ultrafast proton motion within the cation in both H_2 and CH_4. We note that the nuclear autocorrelation function is a sensitive measure of nuclear wavepacket decoherence. In more recent work (Johnson et al., 2018) a retrieval algorithm was developed based on comparing spectra recorded over a range of intensities, a procedure that systematically changed the chirp mapping and so allowed non-dynamical factors to be eliminated. This has been used to measure very fast nuclear wavepacket decoherence times in the benzene cation with timescales of ≈ 4 fs.

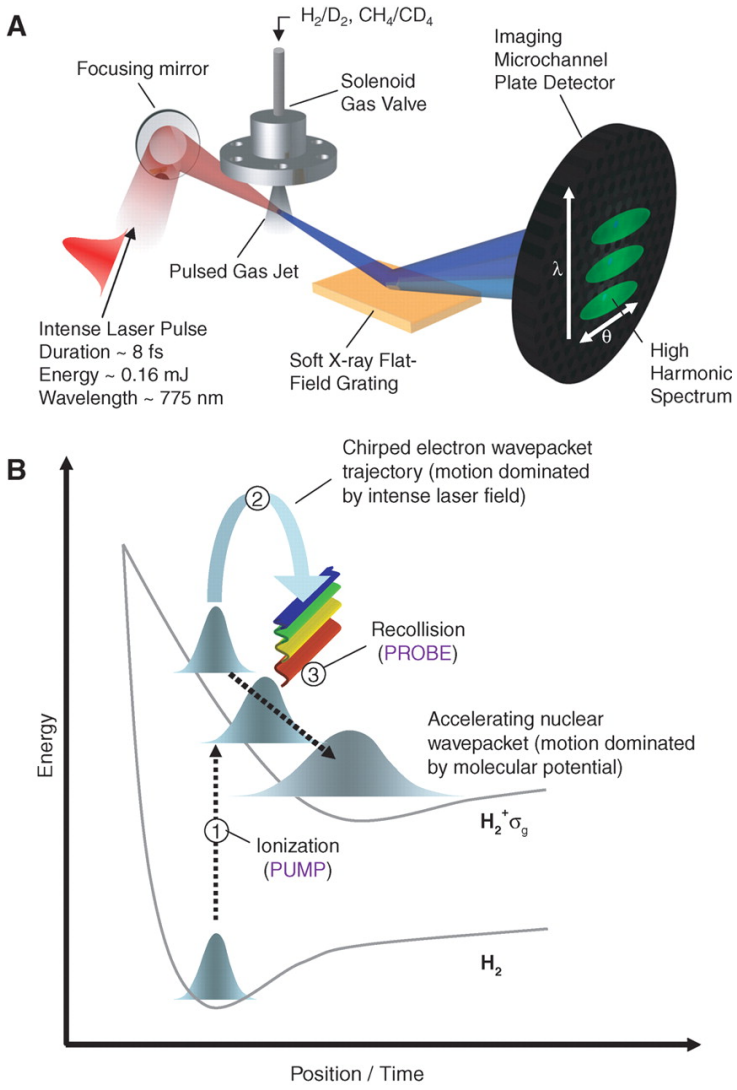

Figure 10: HHG based pump-probe method for measuring proton dynamics in molecules. (a) The experimental setup required to observe high-harmonic emission. (b) Field induced ionization serves as the pump and it launches an electron wavepacket into the continuum simultaneously with a nuclear wavepacket on the cationic ground state potential surface. The electron wavepacket then moves in response to the laser field, returning to the parent ion with an increased kinetic energy at some later time. The length of the return time (pump-probe delay) is encoded in the kinetic energy of the returning electron. The recollision acts as the probe of the nuclear motion that has occurred in the time delay since ionization occurred. Adapted from (Baker et al., 2006) with permission from AAAS.

6. Quantum control and the concept of charge-directed reactivity

The idea that unimolecular chemical reactions might be manipulated through control of electronic wavepackets dates back from experiments at the end of the 90s where fragmentation in small polypeptides was believed to be controlled by the dynamics of a superposition of quasi-degenerate electronic states (Weinkauf et al., 1996, 1997). The interpretation of such coupled electron-nuclear dynamics has however proven to be difficult. With the technological advances of attoscience, the concept of *charge-directed reactivity* has recently been revisited, experimentally and theoretically, mostly on diatomic molecules (Roudnev et al., 2004; Kling et al., 2006, 2013; Nikodem et al., 2017). For instance, the control of electron localisation during dissociative ionisation has been demonstrated in H_2 and its isotopes (Roudnev et al., 2004; Kling et al., 2006). The relative phase of the coherent superposition of the two lowest electronic states, controlled by the phase of the electric field at the time of ionisation, determines whether the positive charge localises on the left or right atom after dissociation. Similarly, the directional emission of C^+ and O^+ fragments has been controlled in the dissociative ionisation of CO (Znakovskaya et al., 2009). Using grid-based quantum mechanical simulations, similar control of the dissociation of the LiH molecule was computationally demonstrated (Nikodem et al., 2017). The new paradigm of attochemistry is to act directly on the electrons and to use *electronic* coherences to create a new electronic density (see interference term in Eq. (2)) directing the nuclear motion in the desired direction (Cerullo and Vozzi, 2012; Vacher et al., 2015a; Meisner et al., 2015).

With the example of BMA[5,5] molecule used already in subsection 3.2, let us illustrate the concept of charge-directed reactivity by analysing the nuclear motion induced upon ionisation to a superposition of electronic eigenstates and comparing it to the nuclear motion induced by a single electronic state (Vacher et al., 2016a). We are particularly interested in the time evolution of the bond lengths of the two terminal methylene groups. For reference, Figure 11a shows, for the BMA[5,5] molecule, nuclear dynamics simulations started at the equilibrium geometry of the neutral species with only the electronic ground state of the cation populated. The unpaired electron is then delocalised over the two methylene groups and does not evolve significantly with time (there is no pure electron dynamics since a single stationary adiabatic state is initially populated). Initially, the two C=C bond lengths are equal to 1.33 Å (a typical value for a carbon double bond). The average

bond length stretches to 1.42 Å and shortens back to the initial value in approximately 20 fs. The stretching is expected since an electron has been removed from a bonding π orbital. The frequency of C=C stretching is typically in the range of 1640-1680 cm^{-1}, which corresponds to a period of vibration of approximately 20 fs and our simulations are in agreement with this value. Importantly, the difference in bond lengths between the two terminal methylene groups is here null: the stretching is symmetric, as expected since the unpaired electron is equally, i.e. symmetrically, delocalised over the two methylene groups.

Figure 11b shows the nuclear motion induced when a superposition of the two lowest-energy electronic cationic states is initially populated. The black dashed line reminds the reader of the oscillations in the electronic density (with nuclei moving) from Fig. 3a. The average bond length evolves in a similar way to the case of dynamics induced by the electronic ground state solely (Fig. 11a): it stretches and vibrates with a period of 20 fs. The difference in bond lengths between the two methylene groups, however, differs from 0: the stretching is asymmetric. More precisely, the difference in bond lengths oscillates with a period that matches the period of the oscillations in the electronic density. Initially, the electronic density is asymmetric with the unpaired electron (or positive charge) located on the left bond (C1-C2). The nuclei thus react asymmetrically i.e. the left (C1-C2) bond stretches more than the right (C3-C4) bond and the difference in bond length (C3-C4)-(C1-C2) becomes negative. As the unpaired electron migrates to the C3-C4 bond, the process will reverse and the C3-C4 bond will stretch more than the C1-C2 bond. Note that it takes a few fs for the nuclear motion to reverse since it has acquired some kinetic energy. The bond length difference does not just oscillate around 0; there is an overall slower evolution. The oscillations in the bond length difference is an illustration of "charge-directed reactivity": the nuclei always try to adapt to the time-dependent electronic distribution.

Using the example of toluene cation, we have demonstrated how different electronic wavepackets lead to different effective potential energy surfaces Vacher et al. (2015a). More precisely, changing the relative weight of an in-phase superposition of cationic states could control the direction in the branching space, i.e. how much certain bonds are shortened or lengthened and how much of a shearing motion takes place: an equal ratio of states results in initial nuclear motion orthogonal to that of the pure electronic states, along the derivative coupling vector. Our previous study on benzene cation extended this investigation to a complex rotation of diabatic states

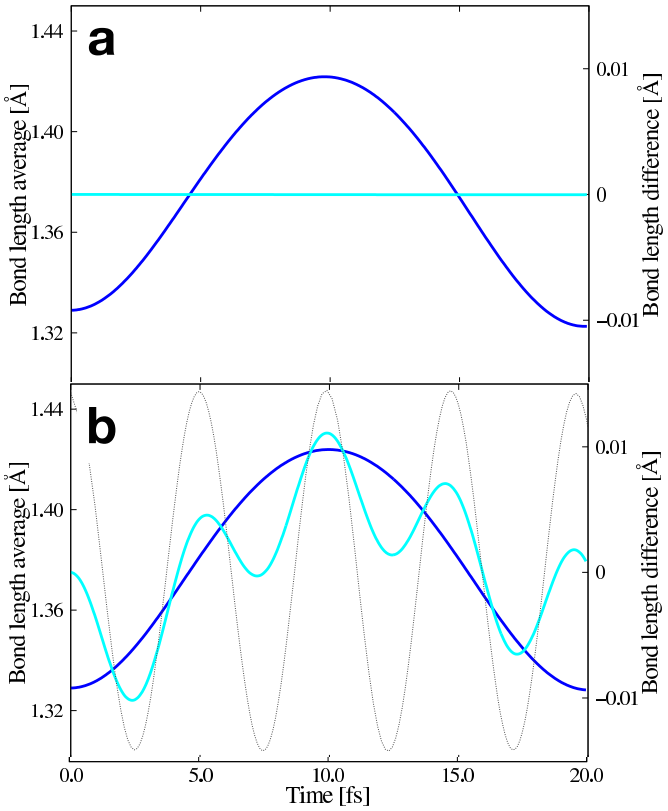

Figure 11: Time evolution of the bond lengths of the two methylene groups (average length of the left (C1–C2) and right (C3–C4) bonds in blue with the left y axis and difference in cyan with the right y axis), upon ionisation of the π system in the BMA[5,5] molecule. The initial electronic state is (**a**) the ground state, (**b**) a coherent superposition of the gound and first electronic cationic states. The scale for the bond length difference is 5 times smaller than for the bond length average. The black dashed line reminds the reader of the oscillations in the electronic density from Fig. 3a. Adapted from (Vacher et al., 2016a) with permission from the Royal Society of Chemistry.

and demonstrated that by modulating the relative weight and phase concurrently both direction and velocity in the full branching space could be controlled (Meisner et al., 2015). By manipulating the composition of the initial electronic wave packet (relative weight and phase) in BMA, one can also manipulate the initial nuclear motion, i.e. which methylene C=C bond stretches more (if any) and by how much (Vacher et al., 2016a). The amplitude and phase of the frequency components of an ultrashort pulse could, in principle, be varied experimentally and will imprint onto the relative weight and phase of the electronic states excited by these frequencies. This methodology provides a route towards coherent electronic control of initial nuclear motion following ionisation or excitation.

Although highly challenging, extending the charge-directed reactivity concept to real chemical reactions in polyatomic molecules is the ambitious goal of attochemistry. Polyatomic molecules contain numerous nuclear coordinates known to lead to electronic decoherence (subsection 3.2), while electronic coherence is a key property for attosecond control. One challenge is thus the following: does electronic coherence or its "legacy" live long enough to affect the outcome of a photochemical reaction? In the example of BMA, as the electron dynamics dephase and the unpaired electron becomes equally delocalised over the two methylene groups, the asymmetry in the stretching of the two π bonds disappears (Vacher et al., 2016a). In the work on glycine (Schwickert et al., 2022) discussed in subsection 5.2 there is evidence that the electronic coherence does couple to vibronic coherence and now there are clues that this may be subject to some general rules (Danilov et al., 2022). A different strategy is to apply a control pulse when the molecular wavepacket approaches the key conical intersection (Hoff et al., 2012; Kling et al., 2013; Schüppel et al., 2020).

In contrast to earlier attempts to control chemical outcomes by selecting vibrational quantum pathways (Shapiro and Brumer, 1985; Tannor and Rice, 1985) where the control was applied on too long a timescale to exploit the fleeting quantum coherence, now it is possible to operate on electronic state superpositions within the decoherence timescale, using the tools of attosecond technology, i.e. few-cycle phase controlled pulses and attosecond XUV/x-ray pulses. Put more directly: if we want to control nuclear dynamics and chemical outcomes, our hypothesis is that we must influence the system before the electronic coherence, and therefore any scope for control, vanishes. Research is underway that targets the control of superposition state evolution by ultrafast light fields in the vicinity of conical intersections, where

strong non-adiabatic electronic-nuclear couplings lead to branching between potential chemical pathways.

Until recently, time-resolved photoexcitation experiments were restricted to following the nuclear motion in what has been termed femtochemistry. State-of-the-art laser spectroscopy techniques, however, can now probe molecular dynamics down to 100 attosecond resolution – the natural timescale of electron motion (Paul et al., 2001; Krausz and Ivanov, 2009). A defining feature of attoscience experiments using few-cycle laser pulses is that a process is initiated by the creation of an electronic wavepacket rather than a nuclear one, due to the large bandwidth of the pulse coherently exciting a set of electronic states. In a number of laboratories it is now possible to address ultrafast excitation through both single and multiphoton channels and follow the earliest dynamics via a range of methodologies such as HHG spectroscopy (Baker et al., 2006), photoelectron and photofragment spectroscopy (Liekhus-Schmaltz et al., 2015; Barillot et al., 2017) and time-resolved X-ray spectroscopy. An excitation-control-probe sequence of pulses synchronised with a precision much finer than the cycle time of the highest frequency optical field can be applied to a selected molecular process. For example, a few-femtosecond UV excitation pulse can initiate the superposition and a few-cycle infrared pulse can then be applied at a short, precisely controlled, delay. Such a pulse sequence can manipulate the coherence between the states, affecting how the system flows through the conical intersection and thus changing the evolution path and final outcomes. Determining the extent to which the coherence is lost between initiation and crossing the intersection will be a key target of both future theory and experimental research. The evolution might be followed via X-ray spectroscopy with sub-femtosecond X-ray pulses, which has a high sensitivity to both structure and electronic states. Computer simulations using state-of-the-art code to solve the coupled nuclear-electronic motion can predict and help interpret such experiments.

This control will be exceptionally challenging to realise because of the ultrafast timescales involved. Nevertheless, with the ultrafast few-cycle optical pulses available to us across the UV-MIR range and attosecond X-ray pulses, we now have the experimental tools to initiate, control and measure these dynamics. The accurate theoretical treatment requires a sophisticated approach with a quantum mechanical treatment of both electron and nuclear dynamics: this is a huge challenge for theory and computation. This enterprise will therefore pioneer new concepts of molecular quantum control that can lead to a deeper understanding of electron-nuclear coupling in

molecules and - eventually - a powerful new array of quantum technologies using quantum dynamics at the fundamental timescales.

7. Future directions of the field

7.1. Emerging attosecond capabilities (XLEAP, angular streaking, nonlinear interactions) and techniques (liquid jets, transmitted spectrum)

In the experimental investigations of attosecond coherent charge dynamics, the systems chosen for investigation and the determined methodology which are judged to be intrinsically interesting are often guided by calculations and by the feasibility of currently available technologies. As methods advance, it becomes possible to investigate a wider range of systems and with greater detail and to investigate previously inaccessible dynamics. We briefly review emerging areas of experimental capability that we see as widening the scope of future investigations.

Interest in charge migration and related phenomena is due to occurrence in nature and application in chemistry. Some of the most important systems and processes will occur in the liquid or solution phase. This has motivated recent efforts to create liquid targets suitable for ultrafast X-ray probing, i.e. of order micron thickens and optically flat. Liquid cells with windows on the order of 100 nm thick have been successfully used for soft X-ray absorption measurements (Meibohm et al., 2014), but are costly to X-ray flux and are unsuitable for most pump-probe measurements due to damage from strong-field pump and very low transmission of UV pumps.

More recently, free-flowing in-vacuum liquid targets have been designed. They each work on a similar principal from fluid dynamics, which has been known since the early work of Taylor (Taylor, 1960). As two equal cylindrical jets collide, their momentum components on the axis of the collision cancel out, and due to the incompressibility of the liquid, symmetric momentum components are produced in orthogonal directions to the plane of collision. The result is a spreading of the liquid into a thin sheet. This can be scaled to micrometer sizes by colliding micrometer cylindrical jets (Ekimova et al., 2015). Other methods of creating the initial transverse momentum can be used, such as using the internal geometry of a nanofabricated nozzle (Galinis et al., 2017), or from channels of high gas pressure (Koralek et al., 2018).

In Section 4 we discussed the practical methods for exciting coherent wavepackets. In particular, due to its feasibility, we focussed on the wavepackets produced by photoionisation. Due to recent advances, we anticipate

that it will soon be possible to excite and measure wavepackets in neutral molecules. XFELs are capable of producing the extreme intensities required for nonlinear X-ray effects. Stimulated X-ray Raman scattering, which is distinct from resonant inelastic Raman scattering (RIXS) as the Stokes transition is itself stimulated, was demonstrated in atomic gasses soon after the development of SASE (Weninger et al., 2013). With the advent of eSASE, coherent bandwidths are available greater than the energy range of the excited states (Duris et al., 2020). They are therefore faster than the response of the system, making impulsive stimulated X-ray Raman scattering possible. Analogously to impulsive Raman in the infrared, which pump or probe vibrational transitions, this could be a powerful tool for studying electron wavepackets (Schweigert and Mukamel, 2007). Compared to direct excitation from a UV source, pumping via X-ray Raman scattering has the additional advantage that the core excited states which form the intermediate pathways for the Raman transitions are highly localised, creating wavepackets localised at specific nuclear sites. Similarly, site specificity when probing state populations via X-ray Raman scattering is expected to provide Angstrom resolution.

Impulsive stimulated X-ray Raman scattering was recently demonstrated in gas phase NO molecules (O'Neal et al., 2020), with valence excitations up to 0.2% detected via excess ionisation with a weak UV pulse. There is still a long way to go before this can be applied to X-ray Raman-pump-Raman-probe experiments. It remains to be seen whether larger excitations can be achieved and whether competing processes of core excitation and ionisation can be suppressed. We anticipate that early experiments will utilise Raman scattering for only one step, for instance to create a wavepacket which is then measured using XAS. It will be difficult to study solid targets, where significant sample damage will be created on a single shot, but liquids, which are self-healing, may be more practical and benefit from propagation effects which enhance Raman sidebands.

Alternatively, excitation of the neutral wavepacket can be achieved by single-photon excitation by a coherent bandwidth spanning the states of the wavepacket, i.e. a few or sub-femtosecond pulse. Valence-excited states are typically between 3 and 6 eV above the ground state, so a UV pulse is required. It has recently become possible to generate few-femtosecond UV pulses through the use of dispersive wave phenomenon in gas-filled hollow-core fibres pumped by few-cycle IR lasers Travers et al. (2019). Many difficulties must be overcome before they can be used in experiments, such as the introduction of low dispersion optics in the UV and the direct character-

isation of these pulses. These challenges do not appear to be fundamental, and we are confident that femtosecond UV pulses will be used in conjunction with either HHG or XFEL sources soon.

Other experimental capabilities are achieved through incremental improvements to methods and apparatus which increase resolution (in energy, time, signal amplitude, etc.) or combine complementary methods for a more complete investigation. Increasing repetition rates, average powers, and stability of HHG sources allow for higher resolution measurements. MHz repetition rates anticipated from XFELs using continuous-wave superconducting RF accelerators will increase average power to unprecedented levels: measurements limited by Poissonian counting statistics which currently take days may be possible in only minutes, allowing for wider and more detailed parametric scans. Advancements in X-ray optics push multiple frontiers, increasing on-target flux, decreasing focal spot sizes, and adding new capabilities such as the possibility to measure incident and transmitted spectra using Fresnel zone plates (Döring et al., 2020).

It is also likely that the field will adapt as new experimental methods are developed. One such method is attosecond angular streaking, also known as the attoclock, which overlaps a circularly polarised IR laser with an X-ray pulse in a gas target and measures the angular (a full revolution) and energy distribution of photoelectrons. The attoclock has been used extensively for the timing of ionisation events (Pfeiffer et al., 2011; Eckle et al., 2008) and more recently for the measurement of X-ray pulses (Hartmann et al., 2018). Because ionisation rates depend on the electronic potential, it is sensitive to the electronic wavefunction. Furthermore, the attoclock can be used to probe the coherence between ionisation pathways (Wickenhauser et al., 2005), and this has been recently used to measure oscillations in the Auger-Meitner decay of a core excited electronic wavepacket (Li et al., 2022). It has the advantage that when measuring Auger decay, the correlation dynamics occur in the neutral molecule, and we anticipate that it may prove successful when applied to measuring excited state dynamics.

7.2. Prospects for, and the importance of, studying attosecond dynamics in larger molecules, biomolecules, condensed phase systems

So far we have considered electronic coherence phenomena (e.g. charge migration) and electron-nuclear coupling (e.g. non-adiabatic coupling at conical intersections, charge density oscillation driven vibronic excitation) only

for relatively small molecular systems. Experimental and theoretical approaches for larger molecules remain in an early stage of development so it is natural to test our ideas on systems more tractable to theoretical computation. Hopefully, over the next few years as we develop the theoretical tools to advance the understanding of the electron nuclear coupling, e.g. ab initio B-spline RCS-ADC method for molecular ionization with the MCTDH scheme for coupled electron-nuclear dynamics, the latter extended to describe general density matrices, will provide a complete quantum-mechanical characterization of the many-body state of atto-ionized molecular systems. This combined with more complete experiments, with improved signal to noise by using higher repetition rate sources and better detection apparatus (e.g. enabling electron-ion coincidence), will further a quantitative understanding of attosecond molecular dynamics in smaller molecules. The benefits of this will be in providing rigorous benchmarking to new computational approaches and in allowing us to understand the photochemistry and photoionization dynamics of atmospheric and astrochemical systems driven by broad-band UV-X-ray radiation.

Looking beyond small gas phase molecular processes we might want to stretch our ambition to understand a wider class of problems around light-driven electronic excitation in molecules and materials. For instance, a key issue in biophysics and in some branches of clinical medicine, is the radiation damage induced by ionising radiation (e.g. UV - X-rays, electrons, ions and other charged particles) to understand the mechanisms and to develop amelioration strategies. In condensed phase systems electronic excitation driven by light underpins a vast array of photochemical (e.g. water-splitting), photophysical (e.g. photovoltaics) and photobiological (e.g. photopharmacological mechanisms) processes and technologies. So far the incisive tools such as time resolved x-ray spectroscopy and scattering with temporal resolution better than 10 femtoseconds to fully understand such processes, especially at the fastest timescales, remain in their infancy. The role of electronic coherence and the critical events in electron-nuclear coupling for this array of processes appears to be a very compelling area for further study.

Before discussing the approaches to research in this area we will briefly consider what the physical issues might be acting in such systems that differ from those at play in small gas phase molecules. For larger molecules we must anticipate increased intra-molecular coupling, for example, a much higher density of electronic states, and of course, far more molecular vibrational modes with which the electronic states may couple. To deal with

this complexity it is likely that a range of measurement methods should be applied to understand the mechanisms across a suite of time and length scales e.g. high temporal resolution x-ray spectroscopy to track local electronic state evolution on a sub 10 fs scale coupled with x-ray and electron scattering studies to track changes to the global structure of the molecule on a longer timescale. For condensed phase systems, e.g. photoexcitations within crystalline dielectric materials, within polymers and for molecules in solution, as well as the increased "intra-molecular" coupling we must anticipate completely new processes arising from the high density environment. For the electronic system these will include modifications to the electronic state energies and character through increased mixing and the influence of Coulombic fields from neighbouring atoms upon the dynamics of charge migration akin to the process of interatomic Coulombic decay. The formation of excitonic states is likely in condensed phase systems and the localisation of these on an ultrafast timescale can play a critical role in charge separation dynamics.

Moreover, the existence of a band-structure within a crystalline lattice will greatly modify the charge transport dynamics. For the nuclear modes we can anticipate in solution phase additional solvent effects, with coupling to the solvent nuclear modes and of steric hindrance in some of the solute nuclear modes.

To progress research on these complex but important problems we must be prepared to use a wide range of tools. On the experimental side the development of new sample environments, e.g. thin polymer films and thin liquid sheets, promises to enable the study of a wide range of systems. In a recent example we have investigated exciton dynamics in thin polymer films. In that work we used HHG based time resolved x-ray spectroscopy (Garratt et al., 2022) at the C K edge following the pumping of an exciton in the organic semiconductor P3HT. A very rapid (10 - 30 fs) delocalisation of excitons, followed by their localisation to a single polymer chain, was observed in these measurements (see Figure 12).

Combining time-resolved x-ray photoelectron and absorption/emission spectroscopy, inelastic resonant x-ray scattering and elastic scattering will all likely have a role in uncovering the complex dynamics. Here the availability of attosecond x-rays will be of critical importance, both from HHG and XFEL based sources. Also crucial will be the use of advanced data analysis techniques including machine learning based approaches to automate the analysis of the pulse x-ray characteristics (Sanchez-Gonzalez et al., 2017),

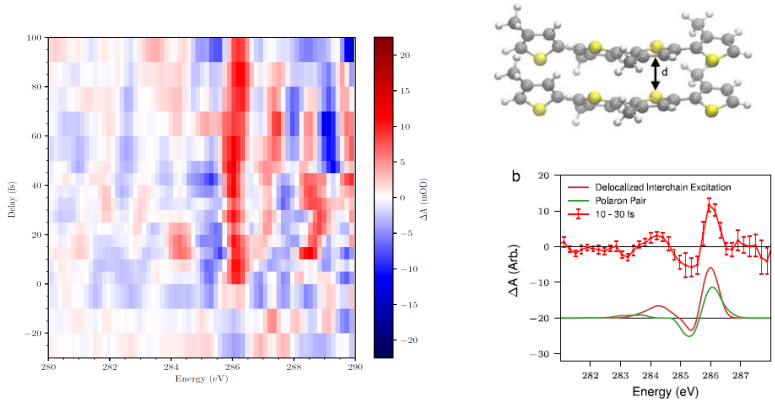

Figure 12: (a)TR-XAS spectrum of P3HT from -30 fs to 100 fs in the vicinity of the carbon K-edge. Note a transient absorption feature at 284.5 eV appearing immediately after pumping and with a lifetime of around 20 fs. (b) A ball and stick model of the simulated tetrathiophene oligomer dimer, showing the π stacking distance, d. (c) A comparison between the differential absorption signal at short time delays (10–30 fs) and the theoretical differential absorption spectrum for a tetrathiophene oligomer dimer, which approximates a delocalized interchain excitation the aggregated polymer which explains the observed temporal dependence of the transient feature at 284.5 eV. In contrast a constrained cationic–anionic tetrathiophene oligomer dimer, which models a polaron pair in the polymer does not offer qualitative agreement with the measured temporal behaviour. Adapted from (Garratt et al., 2022) with permission from Springer Nature.

spectral domain ghost imaging methods (Driver et al., 2020b; Li et al., 2021) and covariance methods. Recent advances in the application of partial covariance analysis of mass-spectra of whole biomolecules (Driver et al., 2020a) are opening up the prospect of a 2-dimensional fragment-fragment correlation capability that could revolutionise the study of the mechanisms of biomolecular fragmentation. This combined with tracking of the key ultrafast electronic events in the fragmentation using pump-probe x-ray spectroscopy can lead to a fuller picture of the role of ultrafast electronic dynamics and electron-nuclear coupling in biomolecular damage by electromagnetic radiation.

7.3. Prospects for, and the importance of, controlling chemistry. Can we control bimolecular reactions?

We have so far considered mono-molecular chemical reactions, i.e. chemical reactions with a single reactant. We may ask whether attochemistry will be relevant for bi-molecular chemical reactions, i.e. chemical reactions between two reactant molecules. Bimolecular photochemical reactions involve the reaction between an electronically excited molecule and a ground state molecule. Those reactions require molecular diffusion and molecular collision. When two molecules collide, their electronic clouds interact and in case of favourable interactions, a stable complex called an "exciplex" is formed. The most common bimolecular photochemical reactions are energy transfer, electron transfer, hydrogen abstraction, etc (Bortolus and Gleria, 1994). For instance, electronic energy transfer is a radiationless process in which the electronic energy initially absorbed by a molecule called a photosensitizer is transferred at a later time to another molecule called a quencher. Another typical example is the 2+2 photocycloaddition reactions, for instance of stilbenes (Lewis, 1986), or indenes (Bortolus and Gleria, 1994). In this class of reactions, two identical or different unsaturated molecules combine with the formation of a cyclic adduct: the resulting reaction is a photo-activated cyclization reaction.

Because bimolecular reactions require that the reactants must diffuse and encounter each other, the kinetics of such processes depends not only on the light–matter interaction but also on the collision rate among the reactants. The excited state need to live long enough to undergo bimolecular reaction with another molecule. This is already a bottleneck in photochemistry and will be all the more true in attochemistry where electronic coherence will need to live long enough to undergo bimolecular reactions. Several strategies have already been proposed to overcome this bottleneck in traditional photochemistry. The simplest approaches are to increase the concentration of solutes in solution to enhance the rate of exciplex formation (eg. photocycloaddition of stilbenes (Lewis, 1986)), or to react with a solvent molecule (eg. reaction of a photoexcited radical with styrene (Koyama and Orr-Ewing, 2016)). Another way to enhance locally the concentration is to use the "cage effect" of dendrimers and confine the solutes in microenvironments (eg. photocycloaddition of acenaphthylene in water-soluble dendritic structures (Kaanumalle et al., 2005)). A different approach is to resort to surface chemistry by co-adsorbing the reactants on the same surface. Examples are CO and NO co-adsorbed with O_2 on Pt(111) to form upon photo-absorption CO_2 and

NO_2, respectively (Mieher and Ho, 1993; Mieher et al., 1996).

These strategies would of course be necessary to apply attosecond science to bimolecular reactions. Whether these would be sufficient to obtain some emergent properties compared to traditional photochemistry remains an outstanding question.

8. Conclusion

In the preceding sections we have discussed our perspective on the attosecond electron dynamics in molecular systems. We present two examples, first two case studies, of experimental evidence where charge migration has been observed in a XAS probe measurement, and where both pump and probe are in the perturbative limit and so not disturbing the intrinsic electronic dynamics. We also identify evidence in the second case study, along with the third case study, where very fast electron-nuclear coupling have been measured. Extensive theoretical work on correlated electronic dynamics and the role of electron-nuclear coupling have been treated is also discussed in section 3. In the latter area we identify that there are two important components to the role of electron-nuclear coupling in charge migration: (i) the intrinsic role of the nuclear wavefunction through the geometry spread of the zero-point energy state that can dephase electronic coherence on time-scales from a few to a few 10's of femtoseconds, (ii) fast nuclear dynamics contributions that are driven by the electronic charge motion and in turn modify that electronic dynamics. We also discuss the competition between coherence and entanglement in a photoionised molecular system (cation + photoelectron) and discuss where entanglement may continue to evolve through the intra-cationic couplings.

We also looked forward to emerging possibilities for attosecond measurement in a more diverse range of molecular systems. This is enabled by a range of new technologies just becoming available, including: (a) higher power and repetition rate high harmonic sources providing attosecond pulses in the XUV, (b) very high power high repetition rate XFEL attosecond pulses, (c) new sample technologies including use of thin films and liquid sheets, (d) an increasing array of measurement methodologies (including coincidence methods, x-ray spectroscopy and x-ray photoelectron spectroscopy) and data analysis methods (e.g. covariance, spectral domain ghost imaging, machine learning). It seems that a much wider range of attosecond time domain dynamics will become accessible to direct measurement over the next

decade.

In parallel advances in theoretical methodology allowing combining of high order electron correlation theory with quantum nuclear dynamics look set to become feasible. We predict a rich seam of work developing these methodologies which will advance quantum chemistry beyond the Born-Oppenheimer approximation. These will improve insight, whilst having high quality experimental data against which to benchmark these advanced quantum chemistry tools. With this validation these tools can be applied to a wide class of photoexcitation problems. We highlight the fundamental connection between exciton dynamics and charge migration that must be operating in organic semiconductors and other extended polymer systems Garratt et al. (2022).

So what is important about this field of research, and why do we foresee that this will continue as an important research area? Firstly, we see that understanding electron-nuclear coupling in molecules is at the core of quantum chemistry: attosecond tests of theoretical understanding and computations will build our knowledge of molecular science beyond the Born-Oppenheimer approximation. Secondly, there are possibilities to implement control via charge directed reactivity that may be of long-term importance to chemical science and technology. Thirdly, in nature photodriven processes (photosynthesis, vision, molecular processes in atmospheric and astrophysical setting) may exhibit the consequences of even the fleeting electronic quantum coherence in their fundamental mechanisms. Fourthly, charge motion is of fundamental importance to our solar energy, electronics and information technologies and how charges move following photoexcitation in condensed media including: organic polymers, semiconductors, conductors and plasmas, might be at the core of some future technologies that drive the clock speeds of electronic and information processing into the peta-Hertz range whilst enhancing efficiencies of photovoltaic materials. This, not necessarily comprehensive list, already motivates the need for further research in this exciting area and we hope others will be motivated to join in this scientific research frontier.

References

Gregory S.J. Armstrong, Margarita A. Khokhlova, Marie Labeye, Andrew S. Maxwell, Emilio Pisanty, and Marco Ruberti. Dialogue on analytical and ab initio methods in attoscience. *European Physical*

Journal D, 75(7):1–31, jul 2021. ISSN 14346079. doi: 10.1140/epjd/s10053-021-00207-3. URL https://link.springer.com/article/10.1140/epjd/s10053-021-00207-3.

Andrew R. Attar, Aditi Bhattacherjee, C. D. Pemmaraju, Kirsten Schnorr, Kristina D. Closser, David Prendergast, and Stephen R. Leone. Femtosecond x-ray spectroscopy of an electrocyclic ring-opening reaction. *Science*, 356(6333):54–59, apr 2017. ISSN 10959203. doi: 10.1126/science.aaj2198. URL https://www.science.org/doi/10.1126/science.aaj2198.

V. Averbukh and M. Ruberti. First-principles Many-electron Dynamics Using the B-spline Algebraic Diagrammatic Construction Approach. In *RSC Theoretical and Computational Chemistry Series*, number 13 in 2018-Janua, pages 68–102. Royal Society of Chemistry, aug 2018. doi: 10.1039/9781788012669-00068. URL https://pubs.rsc.org/en/content/chapter/bk9781782629955-00068/978-1-78262-995-5.

S Baker, J S Robinson, C A Haworth, H Teng, R A Smith, C C Chirila, M Lein, J W G Tisch, and J P Marangos. Probing proton dynamics in molecules on an attosecond time scale. *Science (New York, N.Y.)*, 312 (5772):424–7, apr 2006. ISSN 1095-9203. doi: 10.1126/science.1123904. URL http://www.ncbi.nlm.nih.gov/pubmed/16513942.

T. Barillot, O. Alexander, B. Cooper, T. Driver, D. Garratt, S. Li, A. Al Haddad, A. Sanchez-Gonzalez, M. Agåker, C. Arrell, M. J. Bearpark, N. Berrah, C. Bostedt, J. Bozek, C. Brahms, P. H. Bucksbaum, A. Clark, G. Doumy, R. Feifel, L. J. Frasinski, S. Jarosch, A. S. Johnson, L. Kjellsson, P. Kolorenč, Y. Kumagai, E. W. Larsen, P. Matia-Hernando, M. Robb, J.-E. Rubensson, M. Ruberti, C. Sathe, R. J. Squibb, A. Tan, J. W. G. Tisch, M. Vacher, D. J. Walke, T. J. A. Wolf, D. Wood, V. Zhaunerchyk, P. Walter, T. Osipov, A. Marinelli, T. J. Maxwell, R. Coffee, A. A. Lutman, V. Averbukh, K. Ueda, J. P. Cryan, and J. P. Marangos. Correlation-Driven Transient Hole Dynamics Resolved in Space and Time in the Isopropanol Molecule. *Physical Review X*, 11(3):031048, sep 2021. ISSN 2160-3308. doi: 10.1103/physrevx.11.031048. URL https://link.aps.org/doi/10.1103/PhysRevX.11.031048.

T. R. Barillot, P. Matia-Hernando, D. Greening, D. J. Walke, T. Witting, L. J. Frasinski, J. P. Marangos, and J. W.G. Tisch. Towards XUV pump-probe experiments in the femtosecond to sub-femtosecond regime: New

measurement of the helium two-photon ionization cross-section. *Chemical Physics Letters*, 683:38–42, sep 2017. ISSN 00092614. doi: 10.1016/j.cplett.2017.05.026.

N. Berrah, A. Sanchez-Gonzalez, Z. Jurek, R. Obaid, H. Xiong, R. J. Squibb, T. Osipov, A. Lutman, L. Fang, T. Barillot, J. D. Bozek, J. Cryan, T. J.A. Wolf, D. Rolles, R. Coffee, K. Schnorr, S. Augustin, H. Fukuzawa, K. Motomura, N. Niebuhr, L. J. Frasinski, R. Feifel, C. P. Schulz, K. Toyota, S. K. Son, K. Ueda, T. Pfeifer, J. P. Marangos, and R. Santra. Femtosecond-resolved observation of the fragmentation of buckminsterfullerene following X-ray multiphoton ionization. *Nature Physics*, 15(12): 1279–1283, sep 2019. ISSN 17452481. doi: 10.1038/s41567-019-0665-7. URL `http://www.nature.com/articles/s41567-019-0665-7`.

Max Born, Kun Huang, and M. Lax. Dynamical Theory of Crystal Lattices. *American Journal of Physics*, 23(7):474–474, oct 1955. ISSN 0002-9505. doi: 10.1119/1.1934059. URL `https://ui.adsabs.harvard.edu/abs/1955AmJPh..23..474B/abstract`.

Pietro Bortolus and Mario Gleria. Photochemistry and photophysics of poly(organophosphazenes) and related compounds: A review. II. Bimolecular reactions, jun 1994. ISSN 10530495. URL `https://link.springer.com/article/10.1007/BF01036538`.

J. Breidbach and L. S. Cederbaum. Migration of holes: Formalism, mechanisms, and illustrative applications. *Journal of Chemical Physics*, 118 (9):3983–3996, mar 2003. ISSN 00219606. doi: 10.1063/1.1540618. URL `http://aip.scitation.org/doi/10.1063/1.1540618`.

F Calegari, D Ayuso, A Trabattoni, L Belshaw, S De Camillis, S Anumula, F Frassetto, L Poletto, A Palacios, P Decleva, J B Greenwood, F Martín, and M Nisoli. Ultrafast electron dynamics in phenylalanine initiated by attosecond pulses. *Science*, 346(6207):336–339, oct 2014. ISSN 10959203. doi: 10.1126/science.1254061. URL `http://www.ncbi.nlm.nih.gov/pubmed/25324385`.

L. S. Cederbaum and J. Zobeley. Ultrafast charge migration by electron correlation. *Chemical Physics Letters*, 307(3-4):205–210, jul 1999. ISSN 00092614. doi: 10.1016/S0009-2614(99)00508-4.

Giulio Cerullo and Caterina Vozzi. Coherent Control of Chemical Reactions on the Attosecond Time Scale. *Physics*, 5:243001, 2012. doi: 10.1103/physics.5.138. URL http://link.aps.org/doi/10.1103/Physics.5.138.

Bridgette Cooper, Přemysl Kolorenč, Leszek J Frasinski, Vitali Averbukh, and Jon P Marangos. Analysis of a measurement scheme for ultrafast hole dynamics by few femtosecond resolution X-ray pump-probe Auger spectroscopy. *Faraday Discussions*, 171:93–111, 2014. ISSN 13645498. doi: 10.1039/c4fd00051j.

Don Danilov, Thierry Tran, Michael J. Bearpark, Jon P. Marangos, Graham A. Worth, and Michael A. Robb. How electronic superpositions drive nuclear motion following the creation of a localized hole in the glycine radical cation. *Journal of Chemical Physics*, 156(24):244114, jun 2022. ISSN 10897690. doi: 10.1063/5.0093780. URL https://aip.scitation.org/doi/abs/10.1063/5.0093780.

J. B. Delos and W. R. Thorson. Diabatic and adiabatic representations for atomic collision processes. In *The Journal of Chemical Physics*, number 4 in 70, pages 1774–1790. American Institute of PhysicsAIP, jul 1979. doi: 10.1063/1.437650. URL https://aip.scitation.org/doi/abs/10.1063/1.437650.

V. Despré, A. Marciniak, V. Loriot, M. C.E. Galbraith, A. Rouzée, M. J.J. Vrakking, F. Lépine, and A. I. Kuleff. Attosecond hole migration in benzene molecules surviving nuclear motion. *Journal of Physical Chemistry Letters*, 6(3):426–431, feb 2015. ISSN 19487185. doi: 10.1021/jz502493j. URL https://pubs.acs.org/doi/full/10.1021/jz502493j.

Florian Döring, Benedikt Rösner, Manuel Langer, Adam Kubec, Armin Kleibert, Jörg Raabe, Carlos A. F. Vaz, Maxime Lebugle, and Christian David. Multifocus off-axis zone plates for x-ray free-electron laser experiments. *Optica*, 7(8):1007, aug 2020. ISSN 23342536. doi: 10.1364/optica.398022. URL https://opg.optica.org/viewmedia.cfm?uri=optica-7-8-1007{&}seq=0{&}html=truehttps://opg.optica.org/abstract.cfm?uri=optica-7-8-1007https://opg.optica.org/optica/abstract.cfm?uri=optica-7-8-1007.

M. Drescher, M. Hentschel, R. Kienberger, M. Uiberacker, V. Yakovlev, A. Scrinzi, Th Westerwalbesloh, U. Kleineberg, U. Heinzmann, and F. Krausz. Time-resolved atomic inner-shell spectroscopy. *Nature*, 419 (6909):803–807, oct 2002. ISSN 00280836. doi: 10.1038/nature01143.

Taran Driver, Bridgette Cooper, Ruth Ayers, Rüdiger Pipkorn, Serguei Patchkovskii, Vitali Averbukh, David R Klug, Jon P Marangos, Leszek J Frasinski, and Marina Edelson-Averbukh. Two-Dimensional Partial-Covariance Mass Spectrometry of Large Molecules Based on Fragment Correlations. *Physical Review X*, 10(4), 2020a. ISSN 21603308. doi: 10.1103/PhysRevX.10.041004.

Taran Driver, Siqi Li, Elio G. Champenois, Joseph Duris, Daniel Ratner, Thomas J. Lane, Philipp Rosenberger, Andre Al-Haddad, Vitali Averbukh, Toby Barnard, Nora Berrah, Christoph Bostedt, Philip H. Bucksbaum, Ryan Coffee, Louis F. Dimauro, Li Fang, Douglas Garratt, Averell Gatton, Zhaoheng Guo, Gregor Hartmann, Daniel Haxton, Wolfram Helml, Zhirong Huang, Aaron Laforge, Andrei Kamalov, Matthias F. Kling, Jonas Knurr, Ming Fu Lin, Taran Drive, James P. MacArthur, Jon P. Marangos, Megan Nantel, Adi Natan, Razib Obaid, Jordan T. O'Neal, Niranjan H. Shivaram, Aviad Schori, Peter Walter, Anna Li Wang, Thomas J.A. Wolf, Agostino Marinelli, and James P. Cryan. Attosecond transient absorption spooktroscopy: A ghost imaging approach to ultrafast absorption spectroscopy. *Physical Chemistry Chemical Physics*, 22(5):2704–2712, feb 2020b. ISSN 14639076. doi: 10.1039/c9cp03951a.

Joseph Duris, Siqi Li, Taran Driver, Elio G. Champenois, James P. MacArthur, Alberto A. Lutman, Zhen Zhang, Philipp Rosenberger, Jeff W. Aldrich, Ryan Coffee, Giacomo Coslovich, Franz Josef Decker, James M. Glownia, Gregor Hartmann, Wolfram Helml, Andrei Kamalov, Jonas Knurr, Jacek Krzywinski, Ming Fu Lin, Jon P. Marangos, Megan Nantel, Adi Natan, Jordan T. O'Neal, Niranjan Shivaram, Peter Walter, Anna Li Wang, James J. Welch, Thomas J.A. Wolf, Joseph Z. Xu, Matthias F. Kling, Philip H. Bucksbaum, Alexander Zholents, Zhirong Huang, James P. Cryan, and Agostino Marinelli. Tunable isolated attosecond X-ray pulses with gigawatt peak power from a free-electron laser. *Nature Photonics*, 14(1):30–36, jan 2020. ISSN 17494893. doi: 10.1038/s41566-019-0549-5.

P. Eckle, A. N. Pfeiffer, C. Cirelli, A. Staudte, R. Dörner, H. G. Muller, M. Büttiker, and U. Keller. Attosecond ionization and tunneling delay time measurements in helium. *Science*, 322(5907):1525–1529, dec 2008. ISSN 00368075. doi: 10.1126/science.1163439. URL https://www.science.org/doi/10.1126/science.1163439.

P. Ehrenfest. Bemerkung über die angenäherte Gültigkeit der klassischen Mechanik innerhalb der Quantenmechanik. *Zeitschrift für Physik*, 45(7-8):455–457, jul 1927. ISSN 14346001. doi: 10.1007/BF01329203. URL https://link.springer.com/article/10.1007/BF01329203.

Maria Ekimova, Wilson Quevedo, Manfred Faubel, Philippe Wernet, and Erik T. J. Nibbering. A liquid flatjet system for solution phase soft-x-ray spectroscopy. *Structural Dynamics*, 2(5):054301, sep 2015. ISSN 2329-7778. doi: 10.1063/1.4928715. URL http://aip.scitation.org/doi/10.1063/1.4928715http://aca.scitation.org/doi/10.1063/1.4928715.

P Emma, K Bane, M Cornacchia, Z Huang, H Schlarb, G Stupakov, and D Walz. Femtosecond and Subfemtosecond X-Ray Pulses from a Self-Amplified Spontaneous-Emission–Based Free-Electron Laser. *Physical Review Letters*, 92(7), 2004. ISSN 10797114. doi: 10.1103/PhysRevLett.92.074801.

Gregory S. Engel, Tessa R. Calhoun, Elizabeth L. Read, Tae Kyu Ahn, Tomáš Mančal, Yuan Chung Cheng, Robert E. Blankenship, and Graham R. Fleming. Evidence for wavelike energy transfer through quantum coherence in photosynthetic systems. *Nature*, 446(7137):782–786, apr 2007. ISSN 14764687. doi: 10.1038/nature05678.

Benjamin Erk, Rebecca Boll, Sebastian Trippel, Denis Anielski, Lutz Foucar, Benedikt Rudek, Sascha W. Epp, Ryan Coffee, Sebastian Carron, Sebastian Schorb, Ken R. Ferguson, Michele Swiggers, John D. Bozek, Marc Simon, Tatiana Marchenko, Jochen Küpper, Ilme Schlichting, Joachim Ullrich, Christoph Bostedt, Daniel Rolles, and Artem Rudenko. Imaging charge transfer in iodomethane upon x-ray photoabsorption. *Science*, 345(6194):288–291, jul 2014. ISSN 10959203. doi: 10.1126/science.1253607. URL https://www.science.org/doi/10.1126/science.1253607.

Gediminas Galinis, Jergus Strucka, Jonathan C.T. Barnard, Avi Braun, Roland A Smith, and Jon P Marangos. Micrometer-thickness liquid sheet

jets flowing in vacuum. *Review of Scientific Instruments*, 88(8), 2017. ISSN 10897623. doi: 10.1063/1.4990130. URL https://doi.org/10.1063/1.4990130http://aip.scitation.org/toc/rsi/88/8.

D. Garratt, L. Misiekis, D. Wood, E. W. Larsen, M. Matthews, O. Alexander, P. Ye, S. Jarosch, C. Ferchaud, C. Strüber, A. S. Johnson, A. A. Bakulin, T. J. Penfold, and J. P. Marangos. Direct observation of ultrafast exciton localization in an organic semiconductor with soft X-ray transient absorption spectroscopy. *Nature Communications*, 13(1):1–8, dec 2022. doi: 10.1038/s41467-022-31008-w.

U. Gelius and K. Siegbahn. ESCA studies of molecular core and valence levels in the gas phase. *General Discussions of Faraday Society*, 54(0): 257–268, jan 1972. ISSN 03017249. doi: 10.1039/DC9725400257.

Eleftherios Goulielmakis, Zhi Heng Loh, Adrian Wirth, Robin Santra, Nina Rohringer, Vladislav S. Yakovlev, Sergey Zherebtsov, Thomas Pfeifer, Abdallah M. Azzeer, Matthias F. Kling, Stephen R. Leone, and Ferenc Krausz. Real-time observation of valence electron motion. *Nature*, 466 (7307):739–743, aug 2010. ISSN 00280836. doi: 10.1038/nature09212.

Chunlei Guo, Ming Li, and George N Gibson. Charge asymmetric dissociation induced by sequential and nonsequential strong field ionization. *Physical Review Letters*, 82(12):2492–2495, 1999. ISSN 10797114. doi: 10.1103/PhysRevLett.82.2492.

M. Harmand, R. Coffee, M. R. Bionta, M. Chollet, D. French, D. Zhu, D. M. Fritz, H. T. Lemke, N. Medvedev, B. Ziaja, S. Toleikis, and M. Cammarata. Achieving few-femtosecond time-sorting at hard X-ray free-electron lasers. *Nature Photonics*, 7(3):215–218, feb 2013. ISSN 17494885. doi: 10.1038/nphoton.2013.11. URL https://www.nature.com/articles/nphoton.2013.11.

N. Hartmann, G. Hartmann, R. Heider, M. S. Wagner, M. Ilchen, J. Buck, A. O. Lindahl, C. Benko, J. Grünert, J. Krzywinski, J. Liu, A. A. Lutman, A. Marinelli, T. Maxwell, A. A. Miahnahri, S. P. Moeller, M. Planas, J. Robinson, A. K. Kazansky, N. M. Kabachnik, J. Viefhaus, T. Feurer, R. Kienberger, R. N. Coffee, and W. Helml. Attosecond time-energy

structure of X-ray free-electron laser pulses. *Nature Photonics*, 12(4):215–220, mar 2018. ISSN 17494893. doi: 10.1038/s41566-018-0107-6. URL https://doi.org/10.1038/s41566-018-0107-6.

Philipp Von Den Hoff, Sebastian Thallmair, Markus Kowalewski, Robert Siemering, and Regina De Vivie-Riedle. Optimal control theory - Closing the gap between theory and experiment, oct 2012. ISSN 14639076. URL https://pubs.rsc.org/en/content/articlehtml/2012/cp/c2cp41838jhttps://pubs.rsc.org/en/content/articlelanding/2012/cp/c2cp41838j.

Andrew J. Jenkins, Morgane Vacher, Michael J. Bearpark, and Michael A. Robb. Nuclear spatial delocalization silences electron density oscillations in 2-phenyl-ethyl-amine (PEA) and 2-phenylethyl-N,N-dimethylamine (PENNA) cations. *Journal of Chemical Physics*, 144(10):104110, mar 2016a. ISSN 00219606. doi: 10.1063/1.4943273. URL http://aip.scitation.org/doi/10.1063/1.4943273.

Andrew J. Jenkins, Morgane Vacher, Rebecca M. Twidale, Michael J. Bearpark, and Michael A. Robb. Charge migration in polycyclic norbornadiene cations: Winning the race against decoherence. *Journal of Chemical Physics*, 145(16):164103, oct 2016b. ISSN 00219606. doi: 10.1063/1.4965436. URL http://aip.scitation.org/doi/10.1063/1.4965436.

Allan S. Johnson, Dane R. Austin, David A. Wood, Christian Brahms, Andrew Gregory, Konstantin B. Holzner, Sebastian Jarosch, Esben W. Larsen, Susan Parker, Christian S. Strüber, Peng Ye, John W.G. Tisch, and Jon P. Marangos. High-flux soft x-ray harmonic generation from ionization-shaped few-cycle laser pulses. *Science Advances*, 4(5):eaar3761, may 2018. ISSN 23752548. doi: 10.1126/sciadv.aar3761. URL http://advances.sciencemag.org/lookup/doi/10.1126/sciadv.aar3761.

Lakshmi S. Kaanumalle, R. Ramesh, V. S.N.Murthy Maddipatla, Jayaraj Nithyanandhan, Narayanaswamy Jayaraman, and V. Ramamurthy. Dendrimers as photochemical reaction media. Photochemical behavior of unimolecular and bimolecular reactions in water-soluble dendrimers. *Journal of Organic Chemistry*, 70(13):5062–5069, jun 2005. ISSN 00223263. doi: 10.1021/jo0503254. URL https://pubs.acs.org/doi/full/10.1021/jo0503254.

Hyuk Kang, Kang Taek Lee, Boyong Jung, Yeon Jae Ko, and Seong Keun Kim. Intrinsic lifetimes of the excited state of DNA and RNA bases. *Journal of the American Chemical Society*, 124(44):12958–12959, nov 2002. ISSN 00027863. doi: 10.1021/ja027627x. URL https://pubs.acs.org/doi/full/10.1021/ja027627x.

Kwang Je Kim. Three-dimensional analysis of coherent amplification and self-amplified spontaneous emission in free-electron lasers. *Physical Review Letters*, 57(15):1871–1874, 1986. ISSN 00319007. doi: 10.1103/PhysRevLett.57.1871.

Kwang-Je Kim, Zhirong Huang, and Ryan Lindberg. *Synchrotron Radiation and Free-Electron Lasers*. Cambridge University Press, 2017. ISBN 9781107162617. doi: 10.1017/9781316677377. URL https://www.cambridge.org/core/books/synchrotron-radiation-and-freeelectron-lasers/F90638BB364B5A3EF9A78978CE15B1A5.

Yoel Kissin, Marco Ruberti, Přemysl Kolorenč, and Vitali Averbukh. Attosecond pump-attosecond probe spectroscopy of Auger decay. *Physical Chemistry Chemical Physics*, 23(21):12376–12386, jun 2021. ISSN 14639076. doi: 10.1039/d1cp00623a. URL https://pubs.rsc.org/en/content/articlehtml/2021/cp/d1cp00623ahttps://pubs.rsc.org/en/content/articlelanding/2021/cp/d1cp00623a.

M. F. Kling, Ch Siedschlag, A. J. Verhoef, J. I. Khan, M. Schultze, Th Uphues, Y. Ni, M. Uiberacker, M. Drescher, F. Krausz, and M. J.J. Vrakking. Control of electron localization in molecular dissociation. *Science*, 312 (5771):246–248, apr 2006. ISSN 00368075. doi: 10.1126/science.1126259. URL https://www.science.org/doi/10.1126/science.1126259.

Matthias F. Kling, Philipp Von Den Hoff, Irina Znakovskaya, and Regina De Vivie-Riedle. (Sub-)femtosecond control of molecular reactions via tailoring the electric field of light. *Physical Chemistry Chemical Physics*, 15(24):9448–9467, may 2013. ISSN 14639076. doi: 10.1039/c3cp50591j. URL https://pubs.rsc.org/en/content/articlehtml/2013/cp/c3cp50591jhttps://pubs.rsc.org/en/content/articlelanding/2013/cp/c3cp50591j.

Lisa Marie Koll, Laura Maikowski, Lorenz Drescher, Tobias Witting, and M. J. Vrakking. Experimental Control of Quantum-Mechanical Entanglement in an Attosecond Pump-Probe Experiment. *Physical Review Letters*, 128(4), 2022. ISSN 10797114. doi: 10.1103/PhysRevLett.128.043201.

Jake D. Koralek, Jongjin B. Kim, Petr Brůža, Chandra B. Curry, Zhijiang Chen, Hans A. Bechtel, Amy A. Cordones, Philipp Sperling, Sven Toleikis, Jan F. Kern, Stefan P. Moeller, Siegfried H. Glenzer, and Daniel P. DePonte. Generation and characterization of ultrathin free-flowing liquid sheets. *Nature Communications*, 9(1):1353, dec 2018. ISSN 20411723. doi: 10.1038/s41467-018-03696-w. URL `http://www.nature.com/articles/s41467-018-03696-w`.

Daisuke Koyama and Andrew J. Orr-Ewing. Photochemical reaction dynamics of 2,2'-dithiobis(benzothiazole): Direct observation of the addition product of an aromatic thiyl radical to an alkene with time-resolved vibrational and electronic absorption spectroscopy. *Physical Chemistry Chemical Physics*, 18(17):12115–12127, apr 2016. ISSN 14639076. doi: 10.1039/c6cp01290f. URL `https://pubs.rsc.org/en/content/articlehtml/2016/cp/c6cp01290fhttps://pubs.rsc.org/en/content/articlelanding/2016/cp/c6cp01290f`.

Ferenc Krausz and Misha Ivanov. Attosecond physics. *Reviews of Modern Physics*, 81(1):163–234, feb 2009. ISSN 00346861. doi: 10.1103/RevModPhys.81.163. URL `https://link.aps.org/doi/10.1103/RevModPhys.81.163`.

M. Kretschmar, A. Hadjipittas, B. Major, J. Tümmler, I. Will, T. Nagy, M. J. J. Vrakking, A. Emmanouilidou, and B. Schütte. Attosecond investigation of extreme-ultraviolet multi-photon multi-electron ionization. *Optica*, 9(6):639, jun 2022. ISSN 23342536. doi: 10.1364/optica.456596. URL `https://opg.optica.org/viewmedia.cfm?uri=optica-9-6-639{&}seq=0{&}html=truehttps://opg.optica.org/abstract.cfm?uri=optica-9-6-639https://opg.optica.org/optica/abstract.cfm?uri=optica-9-6-639`.

Manuel Lara-Astiaso, Mara Galli, Andrea Trabattoni, Alicia Palacios, David Ayuso, Fabio Frassetto, Luca Poletto, Simone De Camillis, Jason Greenwood, Piero Decleva, Ivano Tavernelli, Francesca Calegari, Mauro Nisoli,

and Fernando Martín. Attosecond Pump-Probe Spectroscopy of Charge Dynamics in Tryptophan. *Journal of Physical Chemistry Letters*, 9(16): 4570–4577, 2018. ISSN 19487185. doi: 10.1021/acs.jpclett.8b01786. URL https://pubs.acs.org/sharingguidelines.

Frederick D Lewis. *Bimolecular Photochemical Reactions of the Stilbenes*, pages 165–235. John Wiley & Sons, Ltd, 1986. ISBN 9780470133439. doi: https://doi.org/10.1002/9780470133439.ch3. URL https://onlinelibrary.wiley.com/doi/abs/10.1002/9780470133439.ch3.

M Lezius, V. Blanchet, Misha Yu Ivanov, and Albert Stolow. Polyatomic molecules in strong laser fields: Nonadiabatic multielectron dynamics. *Journal of Chemical Physics*, 117(4):1575–1588, 2002. ISSN 00219606. doi: 10.1063/1.1487823. URL https://doi.org/10.1063/1.1487823.

Siqi Li, Taran Driver, Oliver Alexander, Bridgette Cooper, Douglas Garratt, Agostino Marinelli, James P. Cryan, and Jonathan P. Marangos. Time-resolved pump-probe spectroscopy with spectral domain ghost imaging. *Faraday Discussions*, 228(0):488–501, may 2021. ISSN 13645498. doi: 10.1039/d0fd00122h.

Siqi Li, Taran Driver, Philipp Rosenberger, Elio G. Champenois, Joseph Duris, Andre Al-Haddad, Vitali Averbukh, Jonathan C.T. Barnard, Nora Berrah, Christoph Bostedt, Philip H. Bucksbaum, Ryan N. Coffee, Louis F. DiMauro, Li Fang, Douglas Garratt, Averell Gatton, Zhaoheng Guo, Gregor Hartmann, Daniel Haxton, Wolfram Helml, Zhirong Huang, Aaron C. LaForge, Andrei Kamalov, Jonas Knurr, Ming Fu Lin, Alberto A. Lutman, James P. MacArthur, Jon P. Marangos, Megan Nantel, Adi Natan, Razib Obaid, Jordan T. O'Neal, Niranjan H. Shivaram, Aviad Schori, Peter Walter, Anna Li Wang, Thomas J.A. Wolf, Zhen Zhang, Matthias F. Kling, Agostino Marinelli, and James P. Cryan. Attosecond coherent electron motion in Auger-Meitner decay. *Science*, 375(6578):285–290, jan 2022. ISSN 10959203. doi: 10.1126/science.abj2096. URL https://www.science.org/doi/10.1126/science.abj2096.

Chelsea E. Liekhus-Schmaltz, Ian Tenney, Timur Osipov, Alvaro Sanchez-Gonzalez, Nora Berrah, Rebecca Boll, Cedric Bomme, Christoph Bostedt, John D. Bozek, Sebastian Carron, Ryan Coffee, Julien Devin, Benjamin

Erk, Ken R. Ferguson, Robert W. Field, Lutz Foucar, Leszek J. Frasinski, James M. Glownia, Markus Gühr, Andrei Kamalov, Jacek Krzywinski, Heng Li, Jonathan P. Marangos, Todd J. Martinez, Brian K. McFarland, Shungo Miyabe, Brendan Murphy, Adi Natan, Daniel Rolles, Artem Rudenko, Marco Siano, Emma R. Simpson, Limor Spector, Michele Swiggers, Daniel Walke, Song Wang, Thorsten Weber, Philip H. Bucksbaum, and Vladimir S. Petrovic. Ultrafast isomerization initiated by X-ray core ionization. *Nature Communications*, 6:1–7, 2015. ISSN 20411723. doi: 10.1038/ncomms9199.

Y. Mairesse, A. De Bohan, L. J. Frasinski, H. Merdji, L. C. Dinu, P. Monchicourt, P. Breger, M. Kovačev, R. Taïeb, B. Carré, H. G. Muller, P. Agostini, and P. Salières. Attosecond Synchronization of High-Harmonic Soft X-rays. *Science*, 302(5650):1540–1543, 2003. ISSN 00368075. doi: 10.1126/science.1090277. URL `http://science.sciencemag.org/content/sci/302/5650/1540.full.pdf`.

Erik P. Månsson, Simone Latini, Fabio Covito, Vincent Wanie, Mara Galli, Enrico Perfetto, Gianluca Stefanucci, Hannes Hübener, Umberto De Giovannini, Mattea C. Castrovilli, Andrea Trabattoni, Fabio Frassetto, Luca Poletto, Jason B. Greenwood, François Légaré, Mauro Nisoli, Angel Rubio, and Francesca Calegari. Real-time observation of a correlation-driven sub 3 fs charge migration in ionised adenine. *Communications Chemistry*, 4(1):1–7, may 2021. ISSN 23993669. doi: 10.1038/s42004-021-00510-5. URL `https://www.nature.com/articles/s42004-021-00510-5`.

Jan Meibohm, Simon Schreck, and Philippe Wernet. Temperature dependent soft x-ray absorption spectroscopy of liquids. *Review of Scientific Instruments*, 85(10):103102, 2014. ISSN 10897623. doi: 10.1063/1.4896977. URL `https://doi.org/10.1063/1.4896977`.

Jan Meisner, Morgane Vacher, Michael J. Bearpark, and Michael A. Robb. Geometric Rotation of the Nuclear Gradient at a Conical Intersection: Extension to Complex Rotation of Diabatic States. *Journal of Chemical Theory and Computation*, 11(7):3115–3122, jun 2015. ISSN 15499626. doi: 10.1021/acs.jctc.5b00364. URL `https://pubs.acs.org/doi/full/10.1021/acs.jctc.5b00364`.

David Mendive-Tapia, Morgane Vacher, Michael J. Bearpark, and Michael A. Robb. Coupled electron-nuclear dynamics: Charge migration and charge

transfer initiated near a conical intersection. *Journal of Chemical Physics*, 139(4):044110, jul 2013. ISSN 00219606. doi: 10.1063/1.4815914. URL https://aip.scitation.org/doi/abs/10.1063/1.4815914.

W. D. Mieher and W. Ho. Bimolecular surface photochemistry: Mechanisms of CO oxidation on Pt(111)at 85 K. *The Journal of Chemical Physics*, 99 (11):9279–9295, aug 1993. ISSN 00219606. doi: 10.1063/1.466209. URL https://aip.scitation.org/doi/abs/10.1063/1.466209.

W. D. Mieher, R. A. Pelak, and W. Ho. Coadsorbate effects in surface photochemistry: Bimolecular reactions and photodesorption yield enhancement for NO coadsorbed with O2 on Pt(111). *Surface Science*, 359(1-3):23–36, jul 1996. ISSN 00396028. doi: 10.1016/0039-6028(96)00372-X.

Astrid Nikodem, R. D. Levine, and F. Remacle. Spatial and temporal control of populations, branching ratios, and electronic coherences in LiH by a single one-cycle infrared pulse. *Physical Review A*, 95(5):053404, may 2017. ISSN 24699934. doi: 10.1103/PhysRevA.95.053404. URL https://journals.aps.org/pra/abstract/10.1103/PhysRevA.95.053404.

M. Nisoli, S. De Silvestri, and O. Svelto. Generation of high energy 10 fs pulses by a new pulse compression technique. *Applied Physics Letters*, 68 (20):2793–2795, may 1996. ISSN 00036951. doi: 10.1063/1.116609. URL http://aip.scitation.org/doi/10.1063/1.116609.

Mauro Nisoli, Piero Decleva, Francesca Calegari, Alicia Palacios, and Fernando Martín. Attosecond Electron Dynamics in Molecules. *Chemical Reviews*, 117(16):10760–10825, aug 2017. ISSN 15206890. doi: 10.1021/acs.chemrev.6b00453. URL https://pubs.acs.org/doi/full/10.1021/acs.chemrev.6b00453.

Jordan T. O'Neal, Elio G. Champenois, Solène Oberli, Razib Obaid, Andre Al-Haddad, Jonathan Barnard, Nora Berrah, Ryan Coffee, Joseph Duris, Gediminas Galinis, Douglas Garratt, James M. Glownia, Daniel Haxton, Phay Ho, Siqi Li, Xiang Li, James Macarthur, Jon P Marangos, Adi Natan, Niranjan Shivaram, Daniel S. Slaughter, Peter Walter, Scott Wandel, Linda Young, Christoph Bostedt, Philip H. Bucksbaum, Antonio Picón, Agostino Marinelli, and James P. Cryan. Electronic Population Transfer via Impulsive Stimulated X-Ray Raman Scattering with Attosecond Soft-X-Ray Pulses. *Physical Review Letters*, 125(7):073203,

aug 2020. ISSN 10797114. doi: 10.1103/PhysRevLett.125.073203. URL https://link.aps.org/doi/10.1103/PhysRevLett.125.073203.

P. M. Paul, E. S. Toma, P. Breger, G. Mullot, F. Augé, Ph Balcou, H. G. Muller, and P. Agostini. Observation of a train of attosecond pulses from high harmonic generation. *Science*, 292(5522):1689–1692, jun 2001. ISSN 00368075. doi: 10.1126/science.1059413. URL http://science.sciencemag.org/.

Adrian N. Pfeiffer, Claudio Cirelli, Mathias Smolarski, Reinhard Dörner, and Ursula Keller. Timing the release in sequential double ionization. *Nature Physics*, 7(5):428–433, mar 2011. ISSN 17452481. doi: 10.1038/nphys1946. URL https://www.nature.com/articles/nphys1946.

A. Picón, C. S. Lehmann, C. Bostedt, A. Rudenko, A. Marinelli, T. Osipov, D. Rolles, N. Berrah, C. Bomme, M. Bucher, G. Doumy, B. Erk, K. R. Ferguson, T. Gorkhover, P. J. Ho, E. P. Kanter, B. Krässig, J. Krzywinski, A. A. Lutman, A. M. March, D. Moonshiram, D. Ray, L. Young, S. T. Pratt, and S. H. Southworth. Hetero-site-specific X-ray pump-probe spectroscopy for femtosecond intramolecular dynamics. *Nature Communications*, 7(1):1–6, may 2016. ISSN 20411723. doi: 10.1038/ncomms11652.

F. Remacle and R. D. Levine. Probing ultrafast purely electronic charge migration in small peptides. *Zeitschrift fur Physikalische Chemie*, 221 (5):647–661, may 2007. ISSN 09429352. doi: 10.1524/zpch.2007.221.5.647. URL https://www.degruyter.com/document/doi/10.1524/zpch.2007.221.5.647/html.

G. W. Richings, I. Polyak, K. E. Spinlove, G. A. Worth, I. Burghardt, and B. Lasorne. Quantum dynamics simulations using Gaussian wavepackets: the vMCG method. *International Reviews in Physical Chemistry*, 34(2):269–308, apr 2015. ISSN 1366591X. doi: 10.1080/0144235X.2015.1051354. URL https://www.tandfonline.com/doi/abs/10.1080/0144235X.2015.1051354.

Berke Vow Ricketti, Erik M. Gauger, and Alessandro Fedrizzi. The coherence time of sunlight in the context of natural and artificial light-harvesting. *Scientific Reports*, 12(1):1–9, dec 2022. ISSN 20452322. doi: 10.1038/s41598-022-08693-0.

Vladimir Roudnev, B D Esry, and I Ben-Itzhak. Controlling HD+ and H2+ dissociation with the carrier-envelope phase difference of an intense ultrashort laser pulse, 2004. ISSN 00319007.

M. Ruberti. Restricted Correlation Space B-Spline ADC Approach to Molecular Ionization: Theory and Applications to Total Photoionization Cross-Sections. *Journal of Chemical Theory and Computation*, 15(6):3635–3653, jun 2019a. ISSN 15499626. doi: 10.1021/acs.jctc.9b00288. URL https://pubs.acs.org/doi/full/10.1021/acs.jctc.9b00288.

M. Ruberti. Onset of ionic coherence and ultrafast charge dynamics in attosecond molecular ionisation. *Physical Chemistry Chemical Physics*, 21 (32):17584–17604, aug 2019b. ISSN 14639076. doi: 10.1039/c9cp03074c. URL https://pubs.rsc.org/en/content/articlehtml/2019/cp/c9cp03074chttps://pubs.rsc.org/en/content/articlelanding/2019/cp/c9cp03074c.

M. Ruberti. Quantum electronic coherences by attosecond transient absorption spectroscopy: Ab initio B-spline RCS-ADC study. *Faraday Discussions*, 228(0):286–311, may 2021. ISSN 13645498. doi: 10.1039/d0fd00104j. URL https://pubs.rsc.org/en/content/articlehtml/2021/fd/d0fd00104jhttps://pubs.rsc.org/en/content/articlelanding/2021/fd/d0fd00104j.

M. Ruberti, R. Yun, K. Gokhberg, S. Kopelke, L. S. Cederbaum, F. Tarantelli, and V. Averbukh. Total molecular photoionization cross-sections by algebraic diagrammatic construction-Stieltjes-Lanczos method: Benchmark calculations. *Journal of Chemical Physics*, 139(14), oct 2013. ISSN 00219606. doi: 10.1063/1.4824431.

M. Ruberti, V. Averbukh, and P. Decleva. B-spline algebraic diagrammatic construction: Application to photoionization cross-sections and high-order harmonic generation. *Journal of Chemical Physics*, 141(16):164126, oct 2014a. ISSN 00219606. doi: 10.1063/1.4900444. URL https://aip.scitation.org/doi/abs/10.1063/1.4900444.

M. Ruberti, R. Yun, K. Gokhberg, S. Kopelke, L. S. Cederbaum, F. Tarantelli, and V. Averbukh. Total photoionization cross-sections of excited electronic states by the algebraic diagrammatic construction-Stieltjes-Lanczos method. *Journal of Chemical Physics*, 140(18):184107, may 2014b. ISSN

00219606. doi: 10.1063/1.4874269. URL https://aip.scitation.org/doi/abs/10.1063/1.4874269.

M. Ruberti, P. Decleva, and V. Averbukh. Full Ab Initio Many-Electron Simulation of Attosecond Molecular Pump-Probe Spectroscopy. *Journal of Chemical Theory and Computation*, 14(10):4991–5000, oct 2018a. ISSN 15499626. doi: 10.1021/acs.jctc.8b00479. URL https://pubs.acs.org/doi/full/10.1021/acs.jctc.8b00479.

M. Ruberti, P. Decleva, and V. Averbukh. Multi-channel dynamics in high harmonic generation of aligned CO2: Ab initio analysis with time-dependent B-spline algebraic diagrammatic construction. *Physical Chemistry Chemical Physics*, 20(12):8311–8325, mar 2018b. ISSN 14639076. doi: 10.1039/c7cp07849h. URL https://pubs.rsc.org/en/content/articlehtml/2018/cp/c7cp07849hhttps://pubs.rsc.org/en/content/articlelanding/2018/cp/c7cp07849h.

Marco Ruberti, Serguei Patchkovskii, and Vitali Averbukh. Quantum coherence in molecular photoionization, aug 2022. ISSN 14639076. URL https://pubs.rsc.org/en/content/articlehtml/2022/cp/d2cp01562ehttps://pubs.rsc.org/en/content/articlelanding/2022/cp/d2cp01562e.

A Sanchez-Gonzalez, P Micaelli, C Olivier, T R Barillot, M Ilchen, A A Lutman, A Marinelli, T Maxwell, A Achner, M Agåker, N Berrah, C Bostedt, J D Bozek, J Buck, P H Bucksbaum, S. Carron Montero, B Cooper, J P Cryan, M Dong, R Feifel, L J Frasinski, H Fukuzawa, A Galler, G. Hartmann, N Hartmann, W Helml, A S Johnson, A Knie, A O Lindahl, J Liu, K Motomura, M Mucke, C. O'Grady, J. E. Rubensson, E R Simpson, R J Squibb, C Såthe, K Ueda, M Vacher, D J Walke, V Zhaunerchyk, R N Coffee, and J P Marangos. Accurate prediction of X-ray pulse properties from a free-electron laser using machine learning. *Nature Communications*, 8, 2017. ISSN 20411723. doi: 10.1038/ncomms15461. URL www.nature.com/naturecommunications.

Jochen Schirmer. *Many-Body Methods for Atoms, Molecules and Clusters*, volume 94 of *Lecture Notes in Chemistry*. Springer International Publishing, Cham, 2018. ISBN 978-3-319-93601-7. doi: 10.1007/978-3-319-93602-4. URL http://link.springer.com/

10.1007/978-3-319-93602-4http://www.springer.com/series/632{%}0Ahttp://link.springer.com/10.1007/978-3-319-93602-4.

Gregory D. Scholes, Graham R. Fleming, Lin X. Chen, Alán Aspuru-Guzik, Andreas Buchleitner, David F. Coker, Gregory S. Engel, Rienk Van Grondelle, Akihito Ishizaki, David M. Jonas, Jeff S. Lundeen, James K. McCusker, Shaul Mukamel, Jennifer P. Ogilvie, Alexandra Olaya-Castro, Mark A. Ratner, Frank C. Spano, K. Birgitta Whaley, and Xiaoyang Zhu. Using coherence to enhance function in chemical and biophysical systems, mar 2017. ISSN 14764687.

E. Schrödinger. An undulatory theory of the mechanics of atoms and molecules. *Physical Review*, 28(6):1049–1070, 1926. ISSN 0031899X. doi: 10.1103/PhysRev.28.1049.

Franziska Schüppel, Thomas Schnappinger, Lena Bäuml, and Regina De Vivie-Riedle. Waveform control of molecular dynamics close to a conical intersection. *Journal of Chemical Physics*, 153(22):224307, dec 2020. ISSN 10897690. doi: 10.1063/5.0031398. URL https://aip.scitation.org/doi/abs/10.1063/5.0031398.

Igor V Schweigert and Shaul Mukamel. Probing valence electronic wavepacket dynamics by all x-ray stimulated Raman spectroscopy: A simulation study. *Physical Review A - Atomic, Molecular, and Optical Physics*, 76(1), 2007. ISSN 10502947. doi: 10.1103/PhysRevA.76.012504.

David Schwickert, Marco Ruberti, Přemysl Kolorenč, Sergey Usenko, Andreas Przystawik, Karolin Baev, Ivan Baev, Markus Braune, Lars Bocklage, Marie Kristin Czwalinna, Sascha Deinert, Stefan Düsterer, Andreas Hans, Gregor Hartmann, Christian Haunhorst, Marion Kuhlmann, Steffen Palutke, Ralf Röhlsberger, Juliane Rönsch-Schulenburg, Philipp Schmidt, Sven Toleikis, Jens Viefhaus, Michael Martins, André Knie, Detlef Kip, Vitali Averbukh, Jon P. Marangos, and Tim Laarmann. Electronic quantum coherence in glycine molecules probed with ultrashort x-ray pulses in real time. *Science Advances*, 8(22):6848, jun 2022. ISSN 23752548. doi: 10.1126/sciadv.abn6848. URL https://www.science.org/doi/10.1126/sciadv.abn6848.

Moshe Shapiro and Paul Brumer. Laser control of product quantum state

populations in unimolecular reactions. *The Journal of Chemical Physics*, 84(7):4103–4104, 1985. ISSN 00219606. doi: 10.1063/1.450074.

E. R. Simpson, A. Sanchez-Gonzalez, D. R. Austin, Z. Diveki, S. E.E. Hutchinson, T. Siegel, M. Ruberti, V. Averbukh, L. Miseikis, C. S. Strüber, L. Chipperfield, and J. P. Marangos. Polarisation response of delay dependent absorption modulation in strong field dressed helium atoms probed near threshold. *New Journal of Physics*, 18(8):083032, aug 2016. ISSN 13672630. doi: 10.1088/1367-2630/18/8/083032. URL https://iopscience.iop.org/article/10.1088/1367-2630/18/8/083032https://iopscience.iop.org/article/10.1088/1367-2630/18/8/083032/meta.

Gero Stibenz, Nickolai Zhavoronkov, and Günter Steinmeyer. Self-compression of millijoule pulses to 78 fs duration in a white-light filament. *Optics Letters*, 31(2):274, jan 2006. ISSN 0146-9592. doi: 10.1364/ol.31.000274.

A Szabo and N L Ostlund. *Modern Quantum Chemistry: {I}ntroduction to Advanced Electronic Structure Theory*. Dover Publications, 1996. URL https://books.google.co.uk/books?hl=en{&}lr={&}id=KQ3DAgAAQBAJ{&}oi=fnd{&}pg=PP1{&}dq=Modern+quantum+chemistry:+Introduction+to+advanced+electronic+structure+theory.{&}ots=P{_}vDOTsfjH{&}sig=NbObJIb924cWLPqDbyPD75YKHaU{&}redir{_}esc=y{#}v=onepage{&}q=Modernquantumchemistry{%}3A.

David J. Tannor and Stuart A. Rice. Control of selectivity of chemical reaction via control of wave packet evolution. *The Journal of Chemical Physics*, 83(10):5013–5018, 1985. ISSN 00219606. doi: 10.1063/1.449767.

G. Taylor. Formation of Thin Flat Sheets of Water. *Proceedings of the Royal Society A: Mathematical, Physical and Engineering Sciences*, 259(1296):1–17, nov 1960. ISSN 1364-5021. doi: 10.1098/rspa.1960.0207. URL http://rspa.royalsocietypublishing.org/cgi/doi/10.1098/rspa.1960.0207.

John C. Travers, Teodora F. Grigorova, Christian Brahms, and Federico Belli. High-energy pulse self-compression and ultraviolet generation through soliton dynamics in hollow capillary fibres. *Nature Photonics*, 13(8):547–554, aug 2019. ISSN 17494893. doi: 10.1038/s41566-019-0416-4.

M. Uiberacker, Th Uphues, M. Schultze, A. J. Verhoef, V. Yakovlev, M. F. Kling, J. Rauschenberger, N. M. Kabachnik, H. Schröder, M. Lezius, K. L. Kompa, H. G. Muller, M. J.J. Vrakking, S. Hendel, U. Kleineberg, U. Heinzmann, M. Drescher, and F. Krausz. Attosecond real-time observation of electron tunnelling in atoms. *Nature*, 446(7136):627–632, apr 2007. ISSN 14764687. doi: 10.1038/nature05648. URL `https://www.nature.com/articles/nature05648`.

Morgane Vacher, Michael J. Bearpark, and Michael A. Robb. Communication: Oscillating charge migration between lone pairs persists without significant interaction with nuclear motion in the glycine and Gly-Gly-NH-CH3 radical cations. *Journal of Chemical Physics*, 140(20): 201102, may 2014a. ISSN 00219606. doi: 10.1063/1.4879516. URL `https://aip.scitation.org/doi/abs/10.1063/1.4879516`.

Morgane Vacher, David Mendive-Tapia, Michael J. Bearpark, and Michael A. Robb. The second-order Ehrenfest method: A practical CASSCF approach to coupled electron-nuclear dynamics. *Theoretical Chemistry Accounts*, 133(7):1–12, jul 2014b. ISSN 1432881X. doi: 10.1007/s00214-014-1505-6. URL `https://link.springer.com/article/10.1007/s00214-014-1505-6`.

Morgane Vacher, Jan Meisner, David Mendive-Tapia, Michael J. Bearpark, and Michael A. Robb. Electronic control of initial nuclear dynamics adjacent to a conical intersection. *Journal of Physical Chemistry A*, 119(21): 5165–5172, may 2015a. ISSN 15205215. doi: 10.1021/jp509774t. URL `https://pubs.acs.org/doi/full/10.1021/jp509774t`.

Morgane Vacher, David Mendive-Tapia, Michael J. Bearpark, and Michael A. Robb. Electron dynamics upon ionization: Control of the timescale through chemical substitution and effect of nuclear motion. *Journal of Chemical Physics*, 142(9):094105, mar 2015b. ISSN 10897690. doi: 10.1063/1.4913515. URL `https://aip.scitation.org/doi/abs/10.1063/1.4913515`.

Morgane Vacher, Lee Steinberg, Andrew J Jenkins, Michael J Bearpark, and Michael A Robb. Electron dynamics following photoionization: Decoherence due to the nuclear-wave-packet width. *Physical Review A - Atomic, Molecular, and Optical Physics*, 92(4):40502, 2015c. ISSN 10941622. doi: 10.1103/PhysRevA.92.040502.

Morgane Vacher, Fabio E.A. Albertani, Andrew J. Jenkins, Iakov Polyak, Michael J. Bearpark, and Michael A. Robb. Electron and nuclear dynamics following ionisation of modified bismethylene-adamantane. In *Faraday Discussions*, volume 194, pages 95–115. Royal Society of Chemistry, dec 2016a. doi: 10.1039/c6fd00067c. URL `https://pubs.rsc.org/en/content/articlehtml/2016/fd/c6fd00067chttps://pubs.rsc.org/en/content/articlelanding/2016/fd/c6fd00067c`.

Morgane Vacher, Michael J. Bearpark, and Michael A. Robb. Direct methods for non-adiabatic dynamics: connecting the single-set variational multi-configuration Gaussian (vMCG) and Ehrenfest perspectives. *Theoretical Chemistry Accounts*, 135(8):1–11, aug 2016b. ISSN 1432881X. doi: 10.1007/s00214-016-1937-2. URL `https://link.springer.com/article/10.1007/s00214-016-1937-2`.

Morgane Vacher, Michael J Bearpark, Michael A Robb, and João Pedro Malhado. Electron Dynamics upon Ionization of Polyatomic Molecules: Coupling to Quantum Nuclear Motion and Decoherence. *Physical Review Letters*, 118(8), 2017. ISSN 10797114. doi: 10.1103/PhysRevLett.118.083001.

Marc J.J. Vrakking. Control of Attosecond Entanglement and Coherence. *Physical Review Letters*, 126(11):113203, 2021. ISSN 10797114. doi: 10.1103/PhysRevLett.126.113203.

R. Weinkauf, P. Schanen, A. Metsala, E. W. Schlag, M. Bürgle, and H. Kessler. Highly efficient charge transfer in peptide cations in the gas phase: Threshold effects and mechanism. *Journal of Physical Chemistry*, 100(47):18567–18585, nov 1996. ISSN 00223654. doi: 10.1021/jp960926m.

R. Weinkauf, E. W. Schlag, T. J. Martinez, and R. D. Levine. Nonstationary electronic states and site-selective reactivity. *Journal of Physical Chemistry A*, 101(42):7702–7710, oct 1997. ISSN 10895639. doi: 10.1021/jp9715742. URL `https://pubs.acs.org/doi/full/10.1021/jp9715742`.

Clemens Weninger, Michael Purvis, Duncan Ryan, Richard A. London, John D. Bozek, Christoph Bostedt, Alexander Graf, Gregory Brown, Jorge J. Rocca, and Nina Rohringer. Stimulated electronic X-ray Raman scattering. *Physical Review Letters*, 111(23):233902, dec 2013. ISSN 00319007. doi: 10.1103/PhysRevLett.111.233902.

Marlene Wickenhauser, Joachim Burgdörfer, Ferenc Krausz, and Markus Drescher. Time resolved fano resonances. *Physical Review Letters*, 94 (2), 2005. ISSN 00319007. doi: 10.1103/PhysRevLett.94.023002.

E. Wigner. On the quantum correction for thermodynamic equilibrium. *Physical Review*, 40(5):749–759, 1932. ISSN 0031899X. doi: 10.1103/PhysRev.40.749.

G. A. Worth, H. D. Meyer, H. Köppel, L. S. Cederbaum, and I. Burghardt. Using the MCTDH wavepacket propagation method to describe multimode non-adiabatic dynamics. *International Reviews in Physical Chemistry*, 27(3):569–606, 2008. ISSN 1366591X. doi: 10.1080/01442350802137656. URL https://www.tandfonline.com/doi/abs/10.1080/01442350802137656.

W. Wurth and D. Menzel. Ultrafast electron dynamics at surfaces probed by resonant Auger spectroscopy. *Chemical Physics*, 251(1-3):141–149, jan 2000. ISSN 03010104. doi: 10.1016/S0301-0104(99)00305-5.

Daehyun You, Kiyoshi Ueda, Marco Ruberti, Kenichi L. Ishikawa, Paolo Antonio Carpeggiani, Tamás Csizmadia, Lénárd Gulyás Oldal, Harshitha N G, Giuseppe Sansone, Praveen Kumar Maroju, Kuno Kooser, Carlo Callegari, Michele Di Fraia, Oksana Plekan, Luca Giannessi, Enrico Allaria, Giovanni De Ninno, Mauro Trov, Laura Badano, Bruno Diviacco, David Gauthier, Najmeh Mirian, Giuseppe Penco, Primož Rebernik Ribič, Simone Spampinati, Carlo Spezzani, Simone Di Mitri, Giulio Gaio, and Kevin C. Prince. A detailed investigation of single-photon laser enabled Auger decay in neon. *New Journal of Physics*, 21(11):113036, nov 2019. ISSN 13672630. doi: 10.1088/1367-2630/ab520d. URL https://iopscience.iop.org/article/10.1088/1367-2630/ab520dhttps://iopscience.iop.org/article/10.1088/1367-2630/ab520d/meta.

Alexander A. Zholents. Method of an enhanced self-amplified spontaneous emission for x-ray free electron lasers. *Physical Review Special Topics - Accelerators and Beams*, 8(4):8–13, apr 2005. ISSN 10984402. doi: 10.1103/PhysRevSTAB.8.040701. URL https://journals.aps.org/prab/abstract/10.1103/PhysRevSTAB.8.040701.

I Znakovskaya, P Von Den Hoff, S Zherebtsov, A Wirth, O Herrwerth, M. J.J. Vrakking, R De Vivie-Riedle, and M F Kling. Attosecond control of elec-

tron dynamics in carbon monoxide. *Physical Review Letters*, 103(10), 2009. ISSN 00319007. doi: 10.1103/PhysRevLett.103.103002.